2. Statistical Properties of Laser Speckle Patterns

J. W. GOODMAN

With 27 Figures

Since speckle plays an important role in many physical phenomena, it is essential to fully understand its statistical properties. Starting from the basic idea of a random walk in the complex plane, we derive the first-order statistics of the complex amplitude, intensity and phase of speckle. Sums of speckle patterns are also considered, the addition being either on an amplitude or on an intensity basis, with partially polarized speckle being a special case. Next we consider the sum of a speckle pattern and a coherent background, deriving the first-order probability density functions of intensity and phase. Attention is then turned to second-order statistics. The autocorrelation function and power spectral density are derived, both for a free-space propagation geometry and for an imaging geometry. In some cases the recorded speckle pattern may be spatially integrated or blurred, and accordingly consideration is given to the statistics of such patterns. Finally, the relationship between detailed surface structure and the resulting speckle pattern is explored, with emphasis on the effects of the surface autocorrelation function and the effects of finite surface roughness.

2.1 Speckle and Its Origins

Operation of the first cw HeNe laser in 1960 revealed an unexpected phenomenon: objects viewed in highly coherent light acquire a peculiar granular appearance. As illustrated in Fig. 2.1, the detailed structure of this granularity bears no obvious relationship to the macroscopic properties of the illuminated object, but rather it appears chaotic and unordered, with an irregular pattern that is best described by the methods of probability theory and statistics.

The physical origin of the observed granularity, which we now know as "laser speckle", was quickly recognized by the early workers in the field (RIGDEN and GORDON [2.1], OLIVER [2.2]). The surfaces of most materials are extremely rough on the scale of an optical wavelength ($\lambda \cong 5 \times 10^{-7}$ meters). When nearly monochromatic light is reflected from such a surface, the optical wave resulting at any moderately

distant point consists of many coherent components or wavelets, each arising from a different microscopic element of the surface. With reference to Fig. 2.2a, the distances travelled by these various wavelets may differ by several or many wavelengths if the surface is truly rough. Interference of the dephased but coherent wavelets results in the granular pattern of intensity that we call speckle.

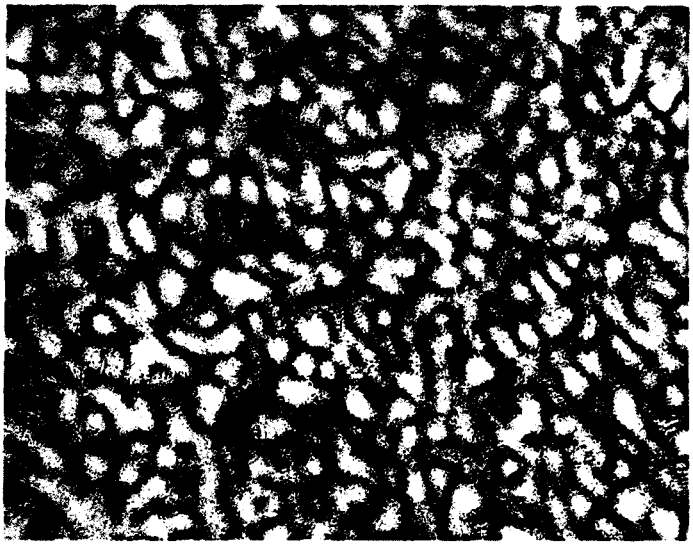

Fig. 2.1. Image of a rough object formed with coherent light

When the geometry is that of an imaging system, rather than the free-space propagation of Fig. 2.2a, the explanation must incorporate diffraction as well as interference. As illustrated in Fig. 2.2b, even for a perfectly corrected (aberration-free) imaging system, the intensity at a given image point can result from the coherent addition of contributions from many independent surface areas. It is necessary only that the diffraction limited (amplitude) point-spread function of the imaging system be broad by comparison with the microscopic surface variations to assure that many de-phased coherent contributions add at each image point. Thus speckle can arise either from free-space propagation of from an imaging operation.

It is now recognized that the basic random interference phenomenon underlying laser speckle has close parallels in many other branches of physics and engineering. Perhaps the earliest mathematical investigations of speckle-like phenomena were those of VERDET [2.3]

and J.W. STRUTT (Lord RAYLEIGH) [2.4], who were concerned with the properties of "coronas", now more commonly known as Fraunhofer rings. Later, in a series of papers dealing with the scattering of light from a large number of particles, LAUE [2.5] derived many basic results that have direct relevance to speckle.

In a more modern vein, direct analogs of laser speckle are found in all types of coherent imagery, including radar astronomy (P. E. GREEN [2.6]), synthetic aperture radar (LEITH [2.7]) and acoustical imagery (P.S. GREEN [2.8]). In addition, statistical phenomena entirely analogous to laser speckle are found in radio-wave propagation (RATCLIFFE [2.9]), temporal statistics of incoherent light (MANDEL [2.10]), theory of narrow-band electrical noise (MIDDLETON [Ref. 2.11, Chap. 9]) and even in the general theory of spectral analysis of random processes (DAVENPORT and ROOT [Ref. 2.12, pp. 107–109]). As a consequence of all these parallels and analogies, the term "speckle" has

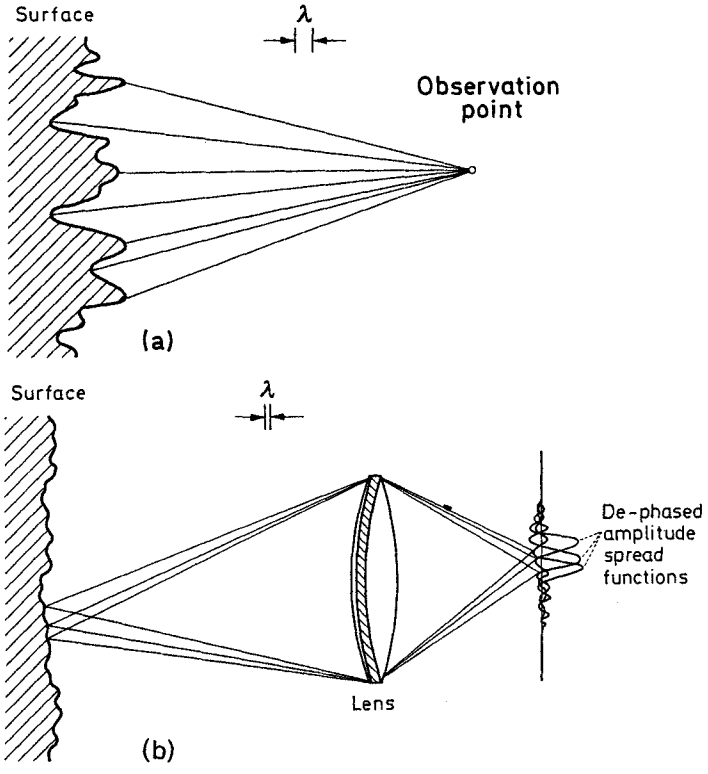

Fig. 2.2a and b. Physical origin of speckle for (a) free-space propagation, (b) an imaging system

taken on a far more general meaning than could have been envisioned when it was first introduced in the 1960's.

The purpose of this chapter is to introduce the various basic statistical properties of speckle patterns. While the context is generally that of *laser* speckle patterns, the results derived apply equally to virtually any coherent random-interference phenomenon, provided the basic underlying statistical assumptions are satisfied (see Subsect. 2.2.1). In some respects, the presentation parallels that of an early report of the author [2.13], unpublished but widely disseminated.[1] In many respects, however, the presentation here is different, a consequence of relative maturity of the field now by comparison with 1963. The reader wishing to acquire a far deeper mathematical understanding of the properties of electromagnetic fields scattered from rough surfaces may wish to consult the standard reference in this field (BECKMANN and SPIZZICHINO [2.14]).

2.2 First-Order Statistics of a Polarized Speckle Pattern

Initially, we limit attention to the first-order statistical properties of speckle, i.e., the statistical properties at a single point in space. Later, in Subsect. 2.5.3, the joint statistical properties of speckle at two or more points will be treated. Throughout this chapter we assume that the waves of concern are perfectly monochromatic, the more general case of polychromatic speckle being treated in Chapter 3. In addition, we consider in this section only the case of a perfectly polarized speckle pattern, the more general case of partially polarized speckle being deferred until Subsect. 2.3.3.

2.2.1 Random Walk in the Complex Plane

Let $u(x,y,z;t)$ be the analytic signal representation of single polarization component of the electric field at observation point (x,y,z) and time instant t. For a monochromatic wave, the analytic signal takes the form

$$u(x,y,z;t) = A(x,y,z)\exp[i2\pi\nu t] \tag{2.1}$$

where ν is the optical frequency, and A represents the phasor amplitude of the field, which is a complex-valued function of space,

$$A(x,y,z) = |A(x,y,z)|\exp[i\theta(x,y,z)]\,. \tag{2.2}$$

[1] The reader may be interested in another early work, the thesis of SCHIFFNER [2.56].

The intensity (irradiance) of the wave is given by

$$I(x,y,z) = \lim_{T\to\infty} \int_{-T/2}^{T/2} |u(x,y,z;t)|^2 \, dt = |A(x,y,z)|^2 \,. \tag{2.3}$$

Whether the speckle pattern arises by free-space propagation or by imaging (c.f. Fig. 2.2), the amplitude of the electric field at a given observation point (x,y) consists of a multitude of de-phased contributions from different scattering regions of the rough surface (for an analysis which treats the surface as a continuum, rather than isolated scattering areas, see Subsect. 2.7). Thus the phasor amplitude $A(x,y,z)$ is represented as a sum of many elementary phasor contributions $(\sqrt{N})^{-1} a_k(x,y,z)$, $k=1,2,\ldots,N$:

$$A(x,y,z) = \sum_{k=1}^{N} \frac{1}{\sqrt{N}} a_k(x,y,z) = \frac{1}{\sqrt{N}} \sum_{k=1}^{N} |a_k| e^{i\phi_k} \,. \tag{2.4}$$

Figure 2.3 illustrates the complex addition of the many elementary phasor contributions to produce the resultant A. We wish to know the statistics (e.g., probability density functions) of the complex field, the intensity, and the phase of the speckle pattern at point (x,y,z). With reference to Fig. 2.3, the problem before us is identical with the classical statistical problem of a random walk in the plane, which has been studied for nearly 100 years [2.4, 15, 16]. We shall derive the necessary results here, being careful to delineate the underlying assumptions and their physical significance.

Let the elementary phasors have the following statistical properties:

(i) The amplitude $a_k/\sqrt{N}$ and the phase ϕ_k of the kth elementary phasor are statistically independent of each other and of the ampli-

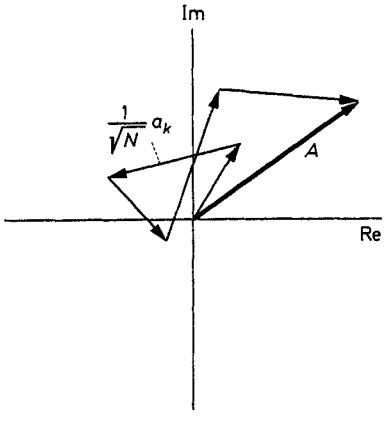

Fig. 2.3. Random walk in the complex plane

tudes and phases of all other elementary phasors (i.e., the elementary scattering areas are unrelated and the strength of a given scattered component bears no relation to its phase);

(ii) The phases ϕ_k are uniformly distributed on the primary interval $(-\pi, \pi)$ (i.e., the surface is rough compared to a wavelength, with the result that phase excursions of many times 2π radians produce a uniform distribution on the primary interval).

With these assumptions, we shall investigate the statistical properties of the resultant complex field.

2.2.2 Statistics of the Complex Amplitude

Attention is now focused on the real and imaginary parts of the resultant field,

$$A^{(r)} \triangleq \mathrm{Re}\{A\} = \frac{1}{\sqrt{N}} \sum_{k=1}^{N} |a_k| \cos \phi_k$$
$$A^{(i)} \triangleq \mathrm{Im}\{A\} = \frac{1}{\sqrt{N}} \sum_{k=1}^{N} |a_k| \sin \phi_k . \tag{2.5}$$

The average values of $A^{(r)}$ and $A^{(i)}$ over an ensemble of macroscopically similar but microscopically different rough surfaces are

$$\langle A^{(r)} \rangle = \frac{1}{\sqrt{N}} \sum_{k=1}^{N} \langle |a_k| \cos \phi_k \rangle = \sum_{k=1}^{N} \langle |a_k| \rangle \langle \cos \phi_k \rangle = 0$$
$$\langle A^{(i)} \rangle = \frac{1}{\sqrt{N}} \sum_{k=1}^{N} \langle |a_k| \sin \phi_k \rangle = \sum_{k=1}^{N} \langle |a_k| \rangle \langle \sin \phi_k \rangle = 0 \tag{2.6}$$

where assumption (i) above is used to average over $|a_k|$ and ϕ_k separately, and assumption (ii) assures a value of zero for $\langle \cos \phi_k \rangle$ and $\langle \sin \phi_k \rangle$. Proceeding in a similar fashion, we see that

$$\langle [A^{(r)}]^2 \rangle = \frac{1}{N} \sum_{k=1}^{N} \sum_{m=1}^{N} \langle |a_k| |a_m| \rangle \langle \cos \phi_k \cos \phi_m \rangle = \frac{1}{N} \sum_{k=1}^{N} \frac{\langle |a_k|^2 \rangle}{2}$$
$$\langle [A^{(i)}]^2 \rangle = \frac{1}{N} \sum_{k=1}^{N} \sum_{m=1}^{N} \langle |a_k| |a_m| \rangle \langle \sin \phi_k \sin \phi_m \rangle = \frac{1}{N} \sum_{k=1}^{N} \frac{\langle |a_k|^2 \rangle}{2}$$
$$\langle A^{(r)} A^{(i)} \rangle = \frac{1}{N} \sum_{k=1}^{N} \sum_{m=1}^{N} \langle |a_k| |a_m| \rangle \langle \cos \phi_k \sin \phi_m \rangle = 0 , \tag{2.7}$$

where we have used the fact that for independent and uniformly distributed phases,

$$\langle \cos\phi_k \cos\phi_m \rangle = \langle \sin\phi_k \sin\phi_m \rangle = \begin{cases} \frac{1}{2} & k = m \\ 0 & k \neq m \end{cases}$$
$$\langle \cos\phi_k \sin\phi_m \rangle = 0 . \tag{2.8}$$

Thus we see that the real and imaginary parts of the complex field have zero means, identical variances, and are uncorrelated.

Now we suppose, as is generally the case in practice, that the number N of elementary phasor contributions is extremely large. Thus the real and imaginary parts of the field are expressed by (2.5) as sums of a very large number of independent random variables. It follows from the central limit theorem [Ref. 2.11, p. 362] that, as $N \to \infty$, $A^{(r)}$ and $A^{(i)}$ are asymptotically Gaussian. Coupling this fact with the results of (2.6) and (2.7), the joint probability density function of the real and imaginary parts of the field is found to asymptotically approach

$$p_{r,i}(A^{(r)}, A^{(i)}) = \frac{1}{2\pi\sigma^2} \exp\left\{ - \frac{[A^{(r)}]^2 + [A^{(i)}]^2}{2\sigma^2} \right\} \tag{2.9}$$

where

$$\sigma^2 = \lim_{N \to \infty} \frac{1}{N} \sum_{k=1}^{N} \frac{\langle |a_k|^2 \rangle}{2} . \tag{2.10}$$

Such a density function is commonly known as a circular Gaussian density function, since contours of constant probability density are circles in the complex plane. Accordingly, the phasor amplitude A is referred to as a circular complex Gaussian random variable.

Some of the modifications that can be made in this argument for the case of a non-uniform distribution of the phases ϕ_k are discussed in Section 2.7. However, in the vast majority of cases of practical interest, the asymptotic results derived above can be used with an extremely high degree of accuracy.

2.2.3 Statistics of Intensity and Phase

For most experiments in the optical region of the spectrum, it is the *intensity* of the wave that is directly measured. Accordingly, from the known statistics of the complex amplitude, we wish to find the corresponding statistical properties of the intensity in a polarized speckle pattern. In addition, the statistical properties of the phase will be found as a by-product of the analysis.

The intensity I and phase θ of the resultant field are related to the real and imaginary parts of the complex amplitude by the transformation

$$\begin{aligned} A^{(r)} &= \sqrt{I}\cos\theta \\ A^{(i)} &= \sqrt{I}\sin\theta, \end{aligned} \tag{2.11}$$

or equivalently by

$$\begin{aligned} I &= [A^{(r)}]^2 + [A^{(i)}]^2 \\ \theta &= \tan^{-1}\frac{A^{(i)}}{A^{(r)}}. \end{aligned} \tag{2.12}$$

To find the joint probability density function of I and θ, we apply the usual techniques for transformations of random variables (see, for example, [Ref. 2.12, p. 32]). The desired joint density function is expressed in terms of the joint density function for $A^{(r)}$ and $A^{(i)}$ as

$$p_{I,\theta}(I,\theta) = p_{r,i}(\sqrt{I}\cos\theta, \sqrt{I}\sin\theta)\|J\| \tag{2.13}$$

where $\|J\|$ is the Jacobian of the transformation

$$\|J\| = \left\| \begin{matrix} \dfrac{\partial A^{(r)}}{\partial I} & \dfrac{\partial A^{(r)}}{\partial \theta} \\ \dfrac{\partial A^{(i)}}{\partial I} & \dfrac{\partial A^{(i)}}{\partial \theta} \end{matrix} \right\| = \tfrac{1}{2} \tag{2.14}$$

and $\|\cdots\|$ symbolizes the modulus of the determinant. Substituting (2.9) in (2.13), we find

$$p_{I,\theta}(I,\theta) = \begin{cases} \dfrac{1}{4\pi\sigma^2}\exp\left(-\dfrac{I}{2\sigma^2}\right) & I \geq 0 \\ & -\pi \leq \theta < \pi \\ 0 & \text{otherwise} \end{cases} \tag{2.15}$$

The marginal probability density function of the intensity alone is found from

$$p_I(I) = \int_{-\pi}^{\pi} p_{I,\theta}(I,\theta)\,d\theta = \begin{cases} \dfrac{1}{2\sigma^2}\exp\left(-\dfrac{I}{2\sigma^2}\right) & I \geq 0 \\ 0 & \text{otherwise}. \end{cases} \tag{2.16}$$

Similarly, the marginal density function of the phase is given by

$$p_\theta(\theta) = \int_{-\pi}^{\pi} p_{I,\theta}(I,\theta)\,dI = \begin{cases} \dfrac{1}{2\pi} & -\pi \le \theta < \pi \\ 0 & \text{otherwise}. \end{cases} \tag{2.17}$$

We conclude that the intensity at a point P in a polarized speckle pattern obeys *negative exponential* statistics, while the phase obeys *uniform* statistics. It should also be noted that

$$p_{I,\theta}(I,\theta) = p_I(I)p_\theta(\theta) \tag{2.18}$$

and hence the intensity and phase are statistically independent at any given point.

Since the intensity is the quantity of primary interest, we investigate its statistical properties in more detail. The nth moment $\langle I^n \rangle$ of intensity is readily shown to be

$$\langle I^n \rangle = n!(2\sigma^2)^n = n!\langle I \rangle^n, \tag{2.19}$$

where we have used the special case $n=1$ to note that the mean value $\langle I \rangle$ is $2\sigma^2$. Of special importance are the second moment and the variance.

$$\begin{aligned} \langle I^2 \rangle &= 2\langle I \rangle^2 \\ \sigma_I^2 &= \langle I^2 \rangle - \langle I \rangle^2 = \langle I \rangle^2 . \end{aligned} \tag{2.20}$$

Thus the standard deviation σ_I of a polarized speckle pattern is equal to the mean intensity. A reasonable measure of the *contrast* of a speckle pattern is the ratio $C = \sigma_I / \langle I \rangle$. Using this definition, we see that the contrast of a polarized speckle pattern is always unity.

In practical applications, it is usually the probability $P(I)$ that the intensity exceeds a threshold I that is of chief interest. In the present case we find that

$$P(I) = \int_I^\infty \frac{1}{\langle I \rangle} \exp\left(-\frac{\xi}{\langle I \rangle} \right) d\xi = \exp(-I/\langle I \rangle). \tag{2.21}$$

Figure 2.4 shows the normalized probability density function $\langle I \rangle p_I(I)$ and the probability that the intensity exceeds a threshold I, $P(I)$. Both functions have the same form in this particular case.

Finally, for purposes of later use, we find the characteristic function of polarized speckle,

$$M_I(iv) = \langle e^{ivI} \rangle = \int_{-\infty}^{\infty} e^{ivI} p_I(I) dI . \tag{2.22}$$

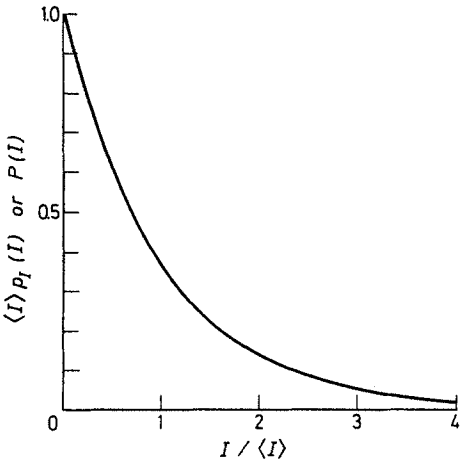

Fig. 2.4. Normalized probability density function and probability that the intensity exceeds level I, for a polarized speckle pattern

For the negative exponential probability density function, the result is readily shown to be

$$M_I(iv) = \frac{1}{1 - iv\langle I \rangle} . \tag{2.23}$$

2.2.4 Experimental Confirmation of the Statistics of Intensity

In the narrow context of laser speckle, the negative exponential probability density function for intensity was first derived by GOODMAN [2.13, 17]. However, entirely equivalent results have been known for more than a century in other contexts (e.g., [2.18]), and have been verified experimentally in those particular fields. The first experimental studies of the intensity statistics of laser speckle were those of CONDIE [2.19], who estimated the cumulative probability distribution $1 - P(I)$ from 120 measurements of intensity. Later, DAINTY [2.20] estimated

probability density functions based on about 2,400 measurements of intensity. In both cases, the estimated statistics agreed with the theory within the accuracy limitations posed by the relatively small numbers of measurements. The most accurate test to date is that of McKechnie [2.21], who made 23,000 measurements of intensity. Figure 2.5 shows his histogram of measured values, together with a negative exponential

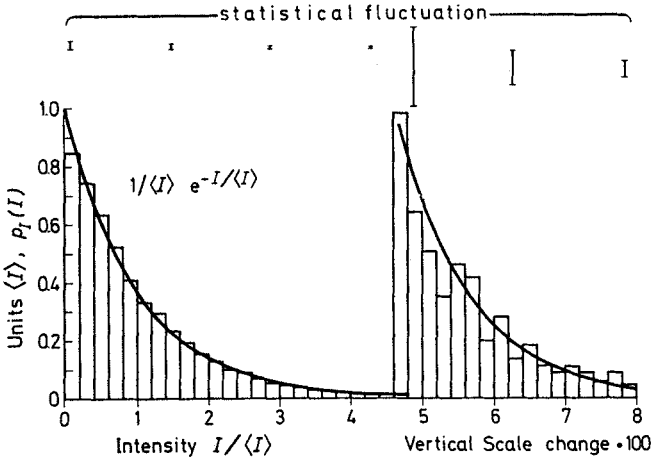

Fig. 2.5. Histogram of the results of 23,000 measurements of speckle intensity [2.21]. Solid line represents a negative exponential distribution

reference curve. The agreement between theory and experiment is excellent, and it seems safe to say that the negative exponential probability density function of polarized laser speckle has been adequately confirmed by experiment.

2.3 First-Order Statistics of Sums of Speckle Patterns

In many experiments, the intensity measured or recorded at a single point in space may be regarded as resulting from a sum of two or more polarized speckle patterns. Such is the case, for example, when the rough surface partially depolarizes the scattered light or when the illuminating beam contains two or more different optical frequencies. Other examples are found in the application of speckle patterns to information processing [2.22] and to interferometry [2.23]; these topics

are discussed in Chapters 5 and 6. Accordingly, this section is devoted to a discussion of the first-order statistics of sums of speckle patterns.

2.3.1 Addition of Speckle Patterns on an Amplitude Basis

Speckle patterns can, in principle, be added on either an amplitude basis or an intensity basis. In practice, the latter is of greater interest, but for completeness we first consider addition on an amplitude basis. As in the previous section, the light is assumed monochromatic and perfectly polarized.

Let the complex field $A(x,y,z)$ result from the addition of N different speckle patterns on an amplitude basis,

$$A = \sum_{k=1}^{N} A_k . \tag{2.24}$$

The individual component fields A_k, being speckle patterns, are zero-mean circular complex Gaussian random variables. The correlation existing between the kth and lth fields is described by the ensemble average $\langle A_k A_l^* \rangle$.

In order to specify the statistics of A, we note that its real (or imaginary) part is a sum of (generally correlated) Gaussian random variables, namely the real (or imaginary) parts of the component fields A_k. Since the sum of any number of real-valued Gaussian random variables (correlated or uncorrelated) is Gaussian, we conclude that the real and imaginary parts of the total field A are Gaussian random variables. In addition, since the real and imaginary parts of each component field A_k have zero means, so too do the real and imaginary parts of the total field A.

At this point we have proved A has real and imaginary parts which are zero-mean Gaussian random variables. We cannot yet conclude, however, that A is a circular complex Gaussian random variable, for we must show that its real and imaginary parts have equal variances and are uncorrelated. This proves to be the case provided the condition

$$\langle A_k A_l \rangle = 0 \quad \text{all } k,l \tag{2.25}$$

is satisfied. Note that the fields can still be correlated ($\langle A_k A_l^* \rangle \neq 0$) even though condition (2.25) is satisfied. In all applications listed above, and in all other applications known to the author, condition 2.25 holds, and hence the total field A is a circular complex Gaussian random variable. It follows that the total intensity $I = |A|^2$ obeys negative exponential statistics, just as the intensities of the component speckle

patterns do. This brings us to the important conclusion that *the addition of speckle patterns on an amplitude basis does not change the statistics of intensity, aside from a scaling constant.*

2.3.2 Addition of Speckle Patterns on an Intensity Basis

We consider next the addition of polarized speckle patterns on an intensity basis, which is the case of greatest practical interest. The approach follows that of GOODMAN [2.24].

Let the total intensity I be composed of a sum of N speckle patterns,

$$I = \sum_{k=1}^{N} I_k \tag{2.26}$$

where $I = |A|^2$ and $I_k = |A_k|^2$. The correlations existing between the N intensity components can be expressed in terms of (real-valued) correlation coefficients

$$c_{kl} = \frac{\langle I_k I_l \rangle - \langle I_k \rangle \langle I_l \rangle}{[\langle (I_k - \langle I_k \rangle)^2 \rangle \langle (I_l - \langle I_l \rangle)^2 \rangle]^{1/2}} . \tag{2.27}$$

Such correlations must of necessity arise from correlations between the underlying fields that give rise to these intensities. The correlation between the kth and lth field components may be written

$$\mu_{kl} = \frac{\langle A_k A_l^* \rangle}{[\langle |A_k|^2 \rangle \langle |A_l|^2 \rangle]^{1/2}} . \tag{2.28}$$

Due to the circular complex Gaussian statistics of the fields, we have the simple relation (c.f. [2.25])

$$\langle I_k I_l \rangle = \langle I_k \rangle \langle I_l \rangle [1 + |\mu_{kl}|^2] \tag{2.29}$$

from which it follows directly that

$$c_{kl} = |\mu_{kl}|^2 . \tag{2.30}$$

Thus the correlation between the kth and lth fields is of the form

$$\mu_{kl} = \sqrt{c_{kl}} \exp(i \psi_{kl}) \tag{2.31}$$

where ψ_{kl} is a phase factor. We shall assume that the full complex correlation coefficients μ_{kl} are known, either through analysis or through experiment.

In order to proceed further, we define an N-element column matrix $[\mathscr{A}]$ with elements $A_1, A_2, \ldots, A_N$,

$$[\mathscr{A}] = \begin{bmatrix} A_1 \\ A_2 \\ \vdots \\ A_N \end{bmatrix}. \tag{2.32}$$

The correlations between the N fields are expressed in most compact form by means of an Hermitian coherency matrix,

$$[\mathscr{J}] = \langle [\mathscr{A}][\mathscr{A}^\dagger] \rangle \tag{2.33}$$

$$= \begin{bmatrix} \langle I_1 \rangle & \sqrt{\langle I_1 \rangle \langle I_2 \rangle}\,\mu_{12} & \cdots & \sqrt{\langle I_1 \rangle \langle I_N \rangle}\,\mu_{1N} \\ \sqrt{\langle I_2 \rangle \langle I_1 \rangle}\,\mu_{12}^* & \langle I_2 \rangle & \cdots & \sqrt{\langle I_2 \rangle \langle I_N \rangle}\,\mu_{2N} \\ \sqrt{\langle I_1 \rangle \langle I_N \rangle}\,\mu_{1N}^* & & \cdots & \langle I_N \rangle \end{bmatrix}$$

where the symbol † indicates an Hermitian transpose operation.

Consider now the effects of a linear transformation on the matrix $[\mathscr{A}]$, represented by an $N \times N$ transformation matrix $[\mathscr{L}]$ and yielding a new matrix $[\mathscr{A}']$,

$$[\mathscr{A}'] = [\mathscr{L}][\mathscr{A}]. \tag{2.34}$$

The coherency matrix $[\mathscr{J}']$ after such a transformation is

$$[\mathscr{J}'] = [\mathscr{L}][\mathscr{J}][\mathscr{L}^\dagger]. \tag{2.35}$$

At this point, we call upon some well-known results of matrix theory [2.26]. For every Hermitian matrix $[\mathscr{J}]$ there exists a unitary transformation matrix $[\mathscr{L}_0]$ which diagonalizes $[\mathscr{J}]$,

$$[\mathscr{J}'] = [\mathscr{L}_0][\mathscr{J}][\mathscr{L}_0^\dagger] = \begin{bmatrix} \lambda_1 & & 0 \\ & \lambda_2 & \\ & & \ddots \\ 0 & & \lambda_N \end{bmatrix}, \tag{2.36}$$

where $\lambda_1, \lambda_2, \ldots, \lambda_N$ are the real and non-negative eigenvalues of $[\mathscr{J}]$. Furthermore, because $[\mathscr{L}_0]$ is unitary (i.e., $[\mathscr{L}_0^\dagger][\mathscr{L}_0]$ equals the identity matrix), the sum of the intensities of the N fields is unchanged by the transformation, for

$$[\mathscr{A}'^\dagger]\,[\mathscr{A}'] = [\mathscr{A}^\dagger][\mathscr{L}_0^\dagger][\mathscr{L}_0][\mathscr{A}] = [\mathscr{A}^\dagger][\mathscr{A}]. \tag{2.37}$$

By applying the transformation $[\mathscr{L}_0]$ to the field-matrix $[\mathscr{A}]$, we have created N new field components $A'_1, A'_2, \ldots, A'_N$ which are *uncorrelated* and which add together on an intensity basis to produce the same total intensity that was present before the transformation, i.e.,

$$I = \sum_{k=1}^{N} |A'_k|^2 = \sum_{k=1}^{N} |A_k|^2 . \tag{2.38}$$

If the condition (2.25) is again satisfied, as it is in all practical cases known to the author, the fields A'_k are zero-mean circular complex random variables. It follows that the intensities $I'_k = |A'_k|^2$ are statistically independent, and each obeys a negative exponential distribution with mean value λ_k,

$$p_{I'_k}(I'_k) = \begin{cases} \dfrac{1}{\lambda_k} \exp\left(-\dfrac{I'_k}{\lambda_k}\right) & I'_k \geq 0 \\ 0 & \text{otherwise.} \end{cases} \tag{2.39}$$

To find the probability density function of the total intensity I, we note that its characteristic function must equal the product of the characteristic functions $M_k(iv)$ of the independent random variables I'_k. Using (2.23), we have

$$M_I(iv) = \prod_{k=1}^{N} (1 - iv\lambda_k)^{-1} . \tag{2.40}$$

The form of the corresponding probability density function of total intensity depends on whether the eigenvalues λ_k are distinct or whether some degeneracy exists. If there exist N non-zero eigenvalues, all of which are distinct, then we have

$$p_I(I) = \sum_{k=1}^{N} \frac{\lambda_k^{N-2}}{\prod\limits_{\substack{p=1 \\ p \neq k}}^{N} (\lambda_k - \lambda_p)} \exp\left(-\frac{I}{\lambda_k}\right) \tag{2.41}$$

for $I \geq 0$, zero otherwise, thus expressing the density function as a sum of simple decaying exponentials. If instead there exist N non-zero eigenvalues, all of which are equal to the single value λ_0, the result is

$$p_I(I) = \frac{I^{N-1}}{(N-1)!\,\lambda_0^N} \exp\left(-\frac{I}{\lambda_0}\right) \tag{2.42}$$

for $I \geq 0$, and zero otherwise. More general cases of clusters of different degenerate eigenvalues can also be handled by standard techniques,

and the density function remains a sum of simple terms. Table 2.1 presents the probability density functions for sums of two and three speckle patterns under all possible conditions of degeneracy.

Table 2.1. Probability density functions of sums of two and three speckle patterns

2 speckle patterns $\lambda_1 \neq \lambda_2$	$p_I(I) = \dfrac{\exp(-I/\lambda_1)}{\lambda_1 - \lambda_2} - \dfrac{\exp(-I/\lambda_2)}{\lambda_1 - \lambda_2}$
2 speckle patterns $\lambda_1 = \lambda_2 = \lambda_0$	$p_I(I) = \dfrac{I}{\lambda_0^2}\exp(-I/\lambda_0)$
3 speckle patterns $\lambda_1 \neq \lambda_2 \neq \lambda_3$	$p_I(I) = \dfrac{\lambda_1}{(\lambda_1-\lambda_2)(\lambda_1-\lambda_3)}\exp(-I/\lambda_1) - \dfrac{\lambda_2}{(\lambda_1-\lambda_2)(\lambda_2-\lambda_3)}\exp(-I/\lambda_2) + \dfrac{\lambda_3}{(\lambda_1-\lambda_3)(\lambda_2-\lambda_3)}\exp(-I/\lambda_3)$
3 speckle patterns $\lambda_1 = \lambda_2 = \lambda_0 \neq \lambda_3$	$p_I(I) = \dfrac{I}{\lambda_0(\lambda_0-\lambda_3)}\exp(-I/\lambda_0) - \dfrac{\lambda_3}{(\lambda_0-\lambda_3)^2}\exp(-I/\lambda_0) + \dfrac{\lambda_3}{(\lambda_0-\lambda_3)^2}\exp(-I/\lambda_3)$
3 speckle patterns $\lambda_1 = \lambda_2 = \lambda_3 = \lambda_0$	$p_I(I) = \dfrac{I^2}{2\lambda_0^3}\exp(-I/\lambda_0)$

In Figure 2.6 are shown the probability density functions for the sum of two speckle patterns for the particular cases of intensity correlation coefficients $c_{12}=0$ ($\lambda_1=\lambda_2=0.5$), $c_{12}=0.6$ ($\lambda_1=0.887$, $\lambda_2=0.113$) and $c_{12}=1.0$ ($\lambda_1=1, \lambda_2=0$), under the assumption that the mean intensities $\langle I_1\rangle$ and $\langle I_2\rangle$ are equal. These curves coincide with those of BARAKAT [2.27], which were found by numerical integration.

When two speckle patterns are added together, the nth moment of the resultant intensity is readily found to be

$$\langle I^n\rangle = n!\,\frac{\lambda_1^{n+1} - \lambda_2^{n+1}}{\lambda_1 - \lambda_2}. \tag{2.43}$$

If the total mean intensity is taken to be unity ($\langle I\rangle=\lambda_1+\lambda_2=1$), the contrast $\sigma_I/\langle I\rangle$ associated with the resultant speckle pattern is readily shown to be

$$C \doteq \frac{\sigma_I}{\langle I\rangle} = [2\lambda_1^2-2\lambda_1+1]^{1/2}. \tag{2.44}$$

This function is plotted in Fig. 2.7. The contrast is seen to reach its minimum value of $1/\sqrt{2}$ when $\lambda_1=\lambda_2=0.5$. More generally, contrast associated with the sum of N speckle patterns assumes a minimum value of $1/\sqrt{N}$ when $\lambda_1=\lambda_2=\cdots=\lambda_N=N^{-1}$.

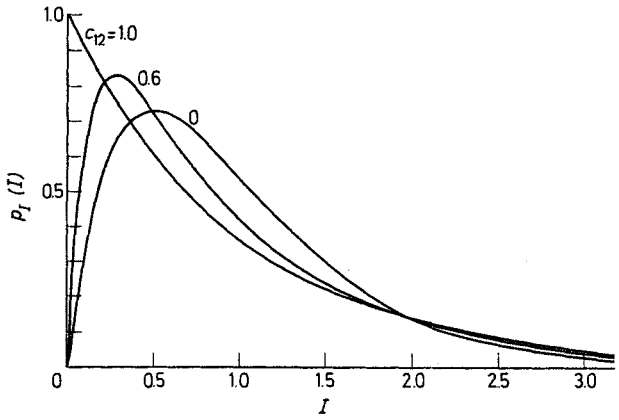

Fig. 2.6. Probability density functions for intensity of the sum of two speckle patterns with $\langle I_1\rangle=\langle I_2\rangle=\frac{1}{2}$ and $c_{12}=0, 0.6, 1.0$

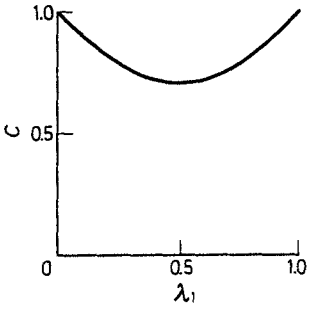

Fig. 2.7. Contrast for sum of two speckle patterns with $\langle I\rangle=1$, plotted as a function of λ_1

For two speckle patterns, the probability $P(I)$ that threshold I is exceeded by the total intensity is found by integrating the appropriate equations in Table 2.1 to be

$$P(I) = \begin{cases} \dfrac{1}{\lambda_1 - \lambda_2} \exp(-I/\lambda_1) - \dfrac{\lambda_2}{\lambda_1 - \lambda_2} \exp(-I/\lambda_2) & \text{for} \quad \lambda_1 \neq \lambda_2 \\ \dfrac{I + \lambda_0}{\lambda_0} \exp(-I/\lambda_0) & \text{for} \quad \lambda_1 = \lambda_2 = \lambda_0 . \end{cases} \tag{2.45}$$

Figure 2.8 shows two plots of $P(I)$ vs. I for the case of unit average intensity ($\lambda_1 + \lambda_2 = 1$).

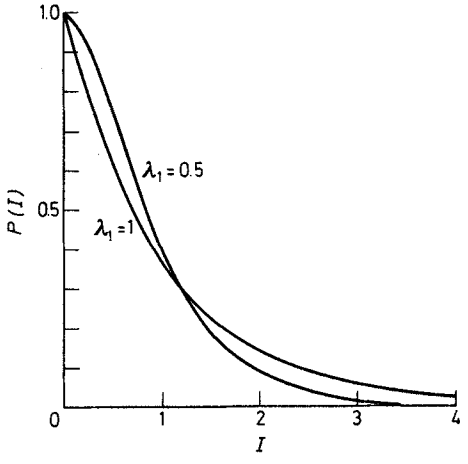

Fig. 2.8. Probability $P(I)$ that intensity value I is exceeded for two speckle patterns, with $\langle I \rangle = 1$. The curves for $\lambda_1 = 0$ and $\lambda_1 = 1$ coincide

The reader should note that, when the original speckle patterns $I_1, I_2, \ldots, I_N$ are uncorrelated at the start, the coherency matrix $[\mathscr{J}]$ is already in diagonal form, and no transformation is required. In this case all previous results can be directly utilized with the simple substitution $\lambda_k = I_k$, $k = 1, 2, \ldots, N$.

2.3.3 Partially Polarized Speckle Patterns

In many experiments, the light scattered from a rough surface may be partially depolarized during the scattering process. Such depolarization is readily observed by allowing the speckle pattern to form through a polarization analyzer. The speckle patterns formed with orthogonal

orientations of the analyzer sometimes appear uncorrelated, sometimes partially correlated.

The speckle pattern formed in the absence of a polarization analyzer may be regarded to be the sum of two speckle patterns, the component patterns arising from orthogonal linearly polarized field components. Thus, having chosen a rectilinear $X-Y$ coordinate system, the total vector field $A(x,y)$ may be written

$$A(x,y) = A_X(x,y)\,l_X + A_Y(x,y)\,l_Y\,, \tag{2.46}$$

where l_X and l_Y are unit vectors in the X- and Y-directions, respectively. The total intensity observed in the speckle pattern is

$$\begin{aligned} I(x,y) &= A(x,y)\cdot A^*(x,y) = |A_X(x,y)|^2 + |A_Y(x,y)|^2 \\ &= I_X(x,y) + I_Y(x,y)\,. \end{aligned} \tag{2.47}$$

Thus the total observed speckle intensity is the sum of two component speckle intensities, each contributed by a different polarization component of the light. These two intensity components are, in general, correlated, and the results of the preceding section must be applied to discover the statistical properties of the total intensity.

Following the approach of WOLF [2.28] and Subsection 2.3.2 (which is a generalization of WOLF's approach), we define the coherency matrix in this case by

$$[\mathscr{J}] = \begin{bmatrix} \langle |A_X|^2 \rangle & \langle A_X A_Y^* \rangle \\ \langle A_X^* A_Y \rangle & \langle |A_Y|^2 \rangle \end{bmatrix}. \tag{2.48}$$

Correlation existing between the two orthogonal polarization components is indicated by non-zero off-diagonal elements of $[\mathscr{J}]$. The coherency matrix can again be diagonalized, in this case by a matrix transformation $[\mathscr{L}_0]$ which is the JONES matrix [2.29] representation of a coordinate rotation, a relative retardation of the two components, or a combination of both. The new coherency matrix becomes

$$[\mathscr{J}'] = \begin{bmatrix} \lambda_1 & 0 \\ 0 & \lambda_2 \end{bmatrix} \tag{2.49}$$

where the eigenvalues λ_1 and λ_2 are given by

$$\lambda_{1,2} = \tfrac{1}{2}\,\mathrm{tr}([\mathscr{J}])\left[1 \pm \sqrt{1 - 4\,\frac{\det([\mathscr{J}])}{(\mathrm{tr}([\mathscr{J}]))^2}}\right], \tag{2.50}$$

where the + and − signs apply for λ_1 and λ_2, respectively, $\mathrm{tr}([\mathscr{J}])$ signifies the trace of $[\mathscr{J}]$ (note since $[\mathscr{L}_0]$ is unitary, $\mathrm{tr}([\mathscr{J}])=\mathrm{tr}([\mathscr{J}'])$ $=\lambda_1+\lambda_2=\langle I\rangle$) and $\det([\mathscr{J}])$ the determinant of $[\mathscr{J}]$.

As first shown by WOLF [2.28], a partially polarized wave can always be represented as the sum of a completely unpolarized wave and a linearly polarized wave. To do so, the diagonalized coherency matrix $[\mathscr{J}']$ is rewritten in the form

$$[\mathscr{J}']=\begin{bmatrix}\lambda_2 & 0\\ 0 & \lambda_2\end{bmatrix}+\begin{bmatrix}\lambda_1-\lambda_2 & 0\\ 0 & 0\end{bmatrix}. \tag{2.51}$$

The first matrix component may be interpreted physically as representing totally unpolarized light with average intensity $2\lambda_2$. The second matrix component represents linearly polarized light with average intensity $\lambda_1-\lambda_2$. The *degree of polarization*, $\mathscr{P}$, of the speckle pattern is defined as the ratio of the average intensity of the polarized component to the total average intensity,

$$\mathscr{P}=\left|\frac{\lambda_1-\lambda_2}{\lambda_1+\lambda_2}\right|=\left[1-4\frac{\det([\mathscr{J}])}{(\mathrm{tr}([\mathscr{J}]))^2}\right]^{1/2}. \tag{2.52}$$

The degree of polarization so defined always lies between zero and one.

The above analysis has demonstrated that a speckle pattern formed in partially polarized light can be regarded in either of two ways. First, it can be regarded as the sum of a polarized speckle pattern and an unpolarized speckle pattern. Second, and more convenient for statistical computations, it can be regarded as the sum of two uncorrelated (and, due to the Gaussian character of the fields, independent) speckle patterns, one with average intensity λ_1 and the second with average intensity λ_2. Expressed in terms of the degree of polarization, these two average intensities are

$$\begin{aligned}\lambda_1&=\tfrac{1}{2}\langle I\rangle(1+\mathscr{P})\\ \lambda_2&=\tfrac{1}{2}\langle I\rangle(1-\mathscr{P}).\end{aligned} \tag{2.53}$$

Using Table 2.1 and (2.53), the probability density function of total intensity takes the form (for $I\geq 0$)

$$p_I(I)=\begin{cases}\dfrac{1}{\langle I\rangle}\exp\left[\dfrac{-2I}{\langle I\rangle(1+\mathscr{P})}\right]-\dfrac{1}{\langle I\rangle}\exp\left[\dfrac{-2I}{\langle I\rangle(1-\mathscr{P})}\right] & \text{for } \mathscr{P}\neq 0\\ \dfrac{4I}{\langle I\rangle^2}\exp\left[-\dfrac{2I}{\langle I\rangle}\right] & \text{for } \mathscr{P}=0.\end{cases} \tag{2.54}$$

The probability $P(I)$ that the intensity exceeds value I is given by

$$P(I)=\begin{cases}\frac{1}{2}(1+\mathscr{P})\exp\left[-\dfrac{2I}{\langle I\rangle(1+\mathscr{P})}\right]-\frac{1}{2}(1-\mathscr{P})\exp\left[-\dfrac{2I}{\langle I\rangle(1-\mathscr{P})}\right] & \text{for } \mathscr{P}\neq 0\\ \dfrac{2I+\langle I\rangle}{\langle I\rangle}\exp\left[-\dfrac{2I}{\langle I\rangle}\right] & \text{for } \mathscr{P}=0\,. \end{cases} \tag{2.55}$$

The curves of Figs. 2.6 and 2.8, which were derived for the sum of two correlated speckle patterns, may also be interpreted as representing results for partially polarized speckle patterns. Figure 2.6 may be regarded as a plot of (2.54) for $\mathscr{P}=0$ ($c_{12}=0$), $\mathscr{P}=0.774$ ($c_{12}=0.6$) and $\mathscr{P}=1$ ($c_{12}=1$), with the general relation $\mathscr{P}=\sqrt{c_{12}}$ between $\mathscr{P}$ and c_{12}. Figure 2.8 shows plots of (2.55) for the cases $\mathscr{P}=0$ ($\lambda_1=0.5$) and $\mathscr{P}=1$ ($\lambda_1=1$).

2.4 First-Order Statistics of the Sum of a Speckle Pattern and a Coherent Background

In a certain class of practical problems, the statistical properties of the sum of a speckle pattern and a coherent background are of interest. These applications include interferometry [2.30] and holography [2.31–33]. Our analysis will be subject to the following assumptions: 1) the speckle pattern is perfectly polarized, with fields that obey circular complex Gaussian statistics, independent of the coherent component; 2) the coherent background is of constant intensity and is co-polarized with the speckle pattern. To the author's knowledge, the more general case of the sum of a partially polarized speckle pattern and a coherent background in an arbitrary polarization state has not been analyzed previously, and the corresponding statistics of the total intensity remain an unsolved problem.

2.4.1 Random Walk plus a Constant Phasor

The speckle pattern may again be visualized as arising from a random walk in the complex plane, with circular Gaussian statistics resulting in the limit of a large number of independent, scattered contributions. To this speckle pattern we add a constant phasor, of known length $\sqrt{I_s}$, and of fixed phase which, without loss of generality, can be taken to be zero degrees (the choice of a phase reference is always at our convenience). Figure 2.9 illustrates the complex sum of interest. We

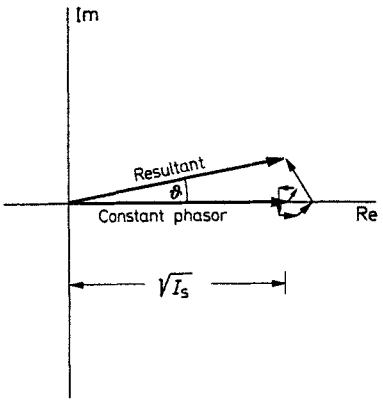

Fig. 2.9. Random walk plus a constant phasor

wish to find the first-order statistical properties of the intensity and phase of the resultant phasor.

The joint statistics of the real and imaginary parts of the field due to the speckle pattern alone are known to be Gaussian (see Eq. (2.9)). The addition of a known phasor with length $\sqrt{I_s}$ and zero phase simply changes the mean value of the real part of the resultant field. Accordingly the joint probability density function of the real and imaginary parts of the total field becomes (c.f., Eq. (2.9))

$$p_{r,i}(A^{(r)}, A^{(i)}) = \frac{1}{2\pi\sigma^2} \exp\left\{ - \frac{[(A^{(r)} - \sqrt{I_s})]^2 + [A^{(i)}]^2}{2\sigma^2} \right\}. \tag{2.56}$$

To find the first-order statistics of the intensity and phase of the resultant, we must apply the transformation of random variables used previously in Subsection 2.2.3.

2.4.2 First-Order Statistics of the Intensity

Using (2.13), (2.14) and (2.56), the joint probability density function of intensity and phase can be written immediately as

$$p_{I,\theta}(I,\theta) = \begin{cases} \dfrac{1}{4\pi\sigma^2} \exp\left(- \dfrac{I + I_s - 2\sqrt{I I_s}\cos\theta}{2\sigma^2} \right) & I \geq 0 \\ & -\pi \leq \theta < \pi \\ 0 & \text{otherwise.} \end{cases} \tag{2.57}$$

The marginal density function for intensity alone is found by integrating the joint density function with respect to θ. Defining $\langle I_N\rangle = 2\sigma^2$ (the mean intensity of the speckle pattern alone) and using the integral identity

$$\int_{-\pi}^{\pi} \exp\left(2\frac{\sqrt{II_s}}{\langle I_N\rangle}\cos\theta\right)d\theta = 2\pi I_0\left(2\frac{\sqrt{II_s}}{\langle I_N\rangle}\right), \tag{2.58}$$

where $I_0(\cdots)$ is a modified Bessel function of the first kind, zero order, we obtain

$$p_I(I) = \begin{cases} \dfrac{1}{\langle I_N\rangle}\exp\left(-\dfrac{I+I_s}{\langle I_N\rangle}\right) I_0\left(2\dfrac{\sqrt{II_s}}{\langle I_N\rangle}\right), & I \geq 0 \\ 0 & \text{otherwise.} \end{cases} \tag{2.59}$$

A similar result was obtained by DAINTY [2.34]. This density function will be referred to as a *modified Rician density*, since it is the density function for the square of a Rician variate (i.e., $\sqrt{I}$ is a Rician random variable). Figure 2.10 shows plots of $\langle I_N\rangle p_I(I)$ vs. $I/\langle I_N\rangle$ for several values of the "beam ratio" parameter $r = I_s/\langle I_N\rangle$.

The moments of the density function (2.59) can be shown to be (c.f. [Ref. 2.11, p. 415])

$$\langle I^n\rangle = n!\,\langle I_N\rangle^n\, {}_1F_1(-n;1;r) \tag{2.60}$$

where ${}_1F_1(a;b;z)$ represents the confluent hypergeometric function. For the special cases $n=1$ and $n=2$, we have

$$\begin{aligned} \langle I\rangle &= \langle I_N\rangle + I_s \\ \langle I^2\rangle &= 2\langle I_N\rangle^2 + 4\langle I_N\rangle I_s + I_s^2. \end{aligned} \tag{2.61}$$

The variance of the total intensity is accordingly

$$\sigma_I^2 = \langle I^2\rangle - \langle I\rangle^2 = \langle I_N\rangle^2(1+2r). \tag{2.62}$$

In many applications, the contrast $\sigma_I/\langle I\rangle$ of the speckle pattern is of prime interest. In this case we have

$$C = \frac{\sqrt{1+2r}}{1+r}, \tag{2.63}$$

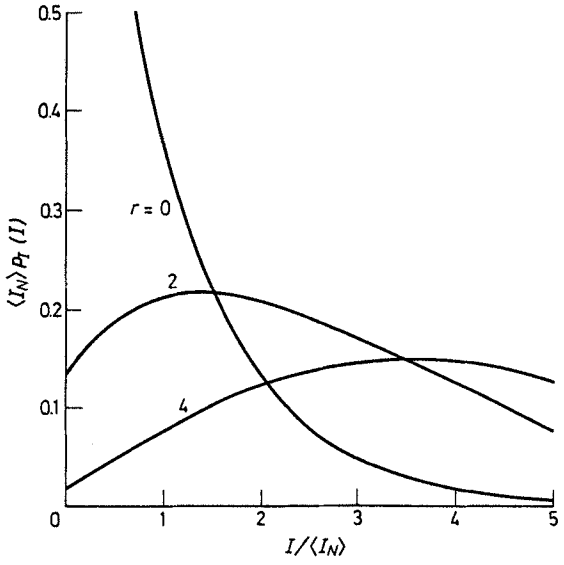

Fig. 2.10. Probability density function of total intensity for a sum of a speckle pattern and a coherent background

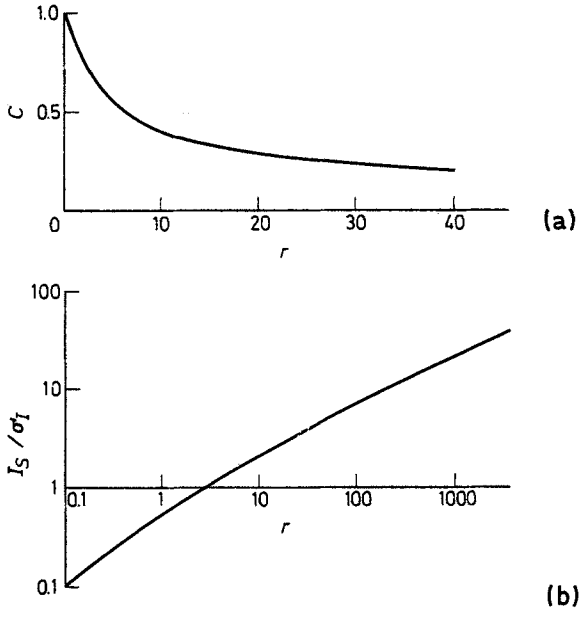

Fig. 2.11 a and b. Dependence of (a) contrast and (b) signal-to-noise ratio on the ratio of background intensity to mean speckle intensity

which is plotted in Fig. 2.11a vs. the beam ratio r. In certain other applications, e.g. [2.31, 33], the "signal-to-noise ratio" I_s/σ_I is of major concern, for which we have

$$\frac{S}{N} = \frac{I_s}{\sigma_I} = \frac{r}{\sqrt{1+2r}}. \tag{2.64}$$

This quantity is plotted in Fig. 2.11b as a function of the beam ratio r. The limiting forms of contrast and signal-to-noise ratio for large and small r are easily seen to be

$$\begin{aligned} \frac{S}{N} &\cong \begin{cases} r & r \ll 1 \\ \sqrt{\frac{r}{2}} & r \gg 1, \end{cases} \\ C &\cong \begin{cases} 1 & r \ll 1 \\ \sqrt{\frac{2}{r}} & r \gg 1. \end{cases} \end{aligned} \tag{2.65}$$

The probability $P(I)$ that the total intensity exceeds value I can be found by integrating the density function (2.59). With the definition $\beta = I/\langle I_N \rangle$, the required integral can be expressed (after a change of variables of integration) as

$$P(I) = \int_{\sqrt{2\beta}}^{\infty} y \exp[-\tfrac{1}{2}(y^2+2r)]\, I_0(\sqrt{2r}\, y)\, dy. \tag{2.66}$$

The integral on the right-hand side can be expressed in terms of tabulated functions known as the Marcum Q-functions [2.35]. In terms of these functions we have

$$P(I) = Q(\sqrt{2r}, \sqrt{2\beta}). \tag{2.67}$$

Figure 2.12 shows plots of $P(I)$ vs. $\beta = I/\langle I_N \rangle$ for several values of beam ratio r.

2.4.3 First-Order Statistics of the Phase

Finally, attention is turned briefly to the first-order statistics of the phase of the sum of a polarized speckle pattern and a coherent background. The probability density function for the phase θ can be found

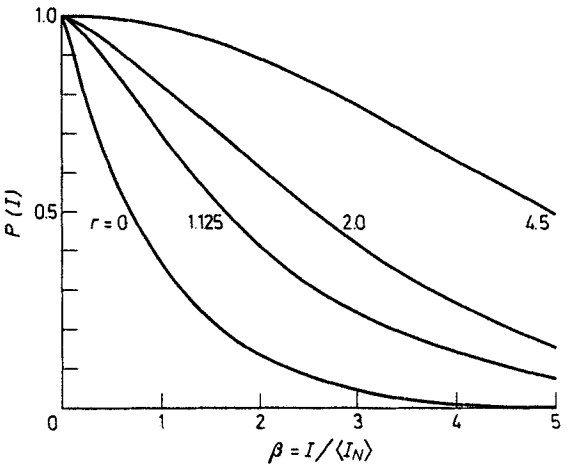

Fig. 2.12. $P(I)$ vs. $I/\langle I_N\rangle$ for several values of $r = I_s/\langle I_N\rangle$

by integrating the joint density function (2.56) with respect to intensity. The integration is a difficult one, but it can be performed and yields [Ref. 2.11, p. 417]

$$p_\theta(\theta) = \frac{e^{-r}}{2\pi} + \sqrt{\frac{r}{\pi}}\cos\theta\cdot\exp(-r\sin^2\theta)\Phi(\sqrt{2r}\cos\theta) \tag{2.68}$$

for $-\pi \leq \theta \leq \pi$, zero otherwise, where

$$\Phi(b) \doteq \frac{1}{\sqrt{2\pi}}\int_{-\infty}^{b} e^{-\frac{y^2}{2}}dy\,. \tag{2.69}$$

A plot of this density function is shown in Fig. 2.13 for several values of the beam ratio r. It can readily be seen from the figure that when the background is very weak ($r \to 0$), the phase of the light becomes uniformly distributed, just as it would be for the speckle pattern alone. When the background is very strong ($r \gg 1$), the density function becomes highly peaked around the phase of the coherent background ($\theta = 0$). When r is large, it can be shown that the density function of the phase is approximately Gaussian,

$$p_\theta(\theta) \cong \sqrt{\frac{r}{\pi}}\exp(-r\theta^2)\,, \tag{2.70}$$

with standard deviation

$$\sigma_\theta \cong \frac{1}{\sqrt{2r}}. \tag{2.71}$$

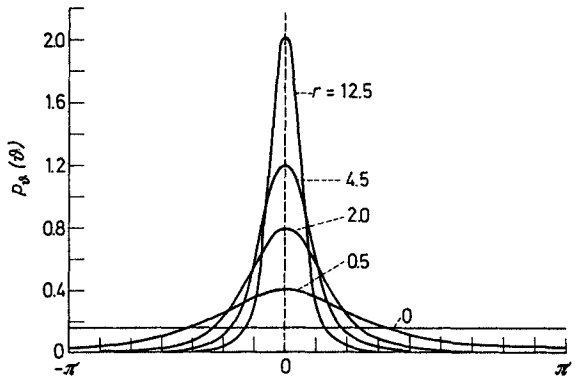

Fig. 2.13. $p_\theta(\theta)$ vs. θ for several values of the parameter $r = I_s/\langle I_N \rangle$ (after MIDDLETON [2.11]).

2.5 Some Second-Order Statistical Properties of Speckle

In previous sections, attention has been limited to the statistical properties of speckle measured at a single point. Such considerations are sufficient to describe the fluctuations of brightness, but are insufficient to describe another fundamental property of speckle—the coarseness of its spatial structure. In this section we accordingly concentrate on the second-order statistics of speckle.

2.5.1 Autocorrelation Function and Power Spectral Density —Free Space Geometry

Consider the free space propagation geometry shown in Fig. 2.14. Monochromatic light is incident on a rough surface, and the scattered light is observed at some distance, without any intervening optical elements. The fields reflected from the rough surface are described in a plane immediately adjacent to that surface by the complex-valued function $\alpha(\xi, \eta)$, representing one linear polarization component of the electric field. The second linear polarization component can be treated

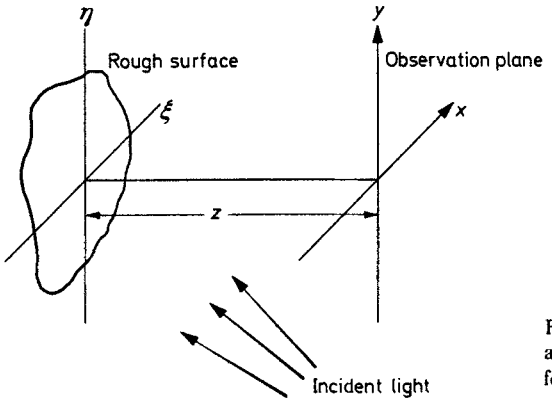

Fig. 2.14. Free-space propagation geometry for speckle formation

(as a first approximation) independently in an identical fashion, but for simplicity we consider a single component.

The complex field $A(x,y)$, observed across a plane parallel with the (ξ,η) plane and at distance z from it, represents the speckle field of interest. We wish to calculate the autocorrelation function of the intensity distribution $I(x,y)=|A(x,y)|^2$ in the (x,y) plane,

$$R_I(x_1,y_1;x_2,y_2)=\langle I(x_1,y_1)I(x_2,y_2)\rangle\,, \tag{2.72}$$

where the average is over an ensemble of rough surfaces. The width of this autocorrelation function provides a reasonable measure of "the average width" of a speckle.

To calculate the autocorrelation function above, we use the fact that for a surface that is rough compared with a wavelength, the field $A(x,y)$ is a circular complex Gaussian random variable at each point (x,y). For such fields, the autocorrelation function of the intensity can be expressed in terms of the autocorrelation function of the fields, which we represent by

$$J_A(x_1,y_1;x_2,y_2)=\langle A(x_1,y_1)A^*(x_2,y_2)\rangle \tag{2.73}$$

and refer to as the *mutual intensity* of the field, in accord with the terminology of coherence theory [2.36]. For circular complex Gaussian fields, the required relation between R_I and J_A is

$$\begin{aligned} R_I(x_1,y_1;x_2,y_2)=&\langle I(x_1,y_1)\rangle\langle I(x_2,y_2)\rangle \\ &+|J_A(x_1,y_1;x_2,y_2)|^2 \end{aligned} \tag{2.74}$$

where we have used the fact that $J_A(x,y;x,y) = \langle I(x,y)\rangle$. The problem of calculating R_I is thus reduced to that of calculating the mutual intensity J_A. It should be re-emphasized that this relationship is valid for surfaces that are rough compared with a wavelength; for smoother surfaces, the fields may not obey circular complex Gaussian statistics (see Sect. 2.7).

Following GOODMAN [2.17] the calculation of the mutual intensity in the observation plane begins with a fundamental relation between the fields $\alpha(\xi,\eta)$ at the scattering surface and the fields $A(x,y)$ in the observation plane. The desired relation is the Huygens-Fresnel principle, expressed in the Fresnel approximation as [Ref. 2.37, Chapt. 4]

$$A(x,y) = \frac{1}{\lambda z}\exp\left[-i\frac{\pi}{\lambda z}(x^2+y^2)\right]\int\int_{-\infty}^{\infty}\alpha(\xi,\eta) \cdot \exp\left[-i\frac{\pi}{\lambda z}(\xi^2+\eta^2)\right]\exp\left[i\frac{2\pi}{\lambda z}(x\xi+y\eta)\right]d\xi\,d\eta\,. \tag{2.75}$$

If $A(x_1,y_1)$ is expressed as such an integral over variables of integration (ξ_1,η_1) and $A(x_2,y_2)$ over variables (ξ_2,η_2), then substitution of these expressions in (2.73), followed by an interchange of orders of integration and averaging yields the following relation between the mutual intensity J_A in the observation region and the mutual intensity J_α in the scattering plane

$$J_A(x_1,y_1;x_2,y_2) = \frac{1}{\lambda^2 z^2}\exp\left[-i\frac{\pi}{\lambda z}(x_1^2-x_2^2+y_1^2-y_2^2)\right] \cdot\int\int\int\int_{-\infty}^{\infty}J_\alpha(\xi_1,\eta_1;\xi_2,\eta_2)\exp\left[-i\frac{\pi}{\lambda z}(\xi_1^2-\xi_2^2+\eta_1^2-\eta_2^2)\right] \cdot\exp\left[i\frac{2\pi}{\lambda z}(x_1\xi_1+y_1\eta_1-x_2\xi_2-y_2\eta_2)\right]d\xi_1\,d\eta_1\,d\xi_2\,d\eta_2\,. \tag{2.76}$$

For the purposes of our present discussion, we make two simplifications in this general relationship. First, since we are concerned here only with the modulus of J_A (c.f., Eq. (2.74)), we drop the initial exponential factor in (x_1,y_1) and (x_2,y_2). Second, we assume that the microstructure of the scattering surface is so fine as to be unresolvable by a lens the size of our observation region in the (x,y) plane, in which case

$$J_\alpha(\xi_1,\eta_1;\xi_2,\eta_2) \cong \kappa P(\xi_1,\eta_1)P^*(\xi_2,\eta_2)\delta(\xi_1-\xi_2,\eta_1-\eta_2) \tag{2.77}$$

where κ is a proportionality constant, the function $P(\xi,\eta)$ represents the amplitude of the field incident on the scattering spot, and $\delta(\xi,\eta)$ is a two-dimensional delta function. (For a more general analysis that does not assume (2.77), see Sect. 2.7.)

The result of these simplifications is

$$J_A(x_1,y_1;x_2,y_2) = \frac{\kappa}{\lambda^2 z^2} \int_{-\infty}^{\infty}\int |P(\xi_1,\eta_1)|^2 \cdot \exp\left\{ i\frac{2\pi}{\lambda z}\left[\xi_1(x_1-x_2)+\eta_1(y_1-y_2)\right]\right\} d\xi_1\, d\eta_1 . \tag{2.78}$$

Thus the mutual intensity of the observed fields depends only on the difference of coordinates in the (x,y) plane, and is given, up to multiplicative constants, by the Fourier transform of the intensity distribution $|P(\xi,\eta)|^2$ incident on the scattering spot. This relation may be regarded as entirely analogous to the Van Cittert-Zernike theorem of classical coherence theory [Ref. 2.38, p. 508].

In many cases, it is convenient to deal with a normalized version of the mutual intensity, known as the *complex coherence factor*, and defined by

$$\mu_A(x_1,y_1;x_2,y_2) \doteq \frac{J_A(x_1,y_1;x_2,y_2)}{[J_A(x_1,y_1;x_1,y_1)J_A(x_2,y_2;x_2,y_2)]^{1/2}} . \tag{2.79}$$

Using (2.78), the complex coherence factor takes the form

$$\mu_A(\Delta x,\Delta y) = \frac{\int_{-\infty}^{\infty}\int |P(\xi,\eta)|^2 \exp\left[i\frac{2\pi}{\lambda z}(\xi\,\Delta x+\eta\,\Delta y)\right] d\xi\, d\eta}{\int_{-\infty}^{\infty}\int |P(\xi,\eta)|^2\, d\xi\, d\eta} . \tag{2.80}$$

Finally, the autocorrelation function of the speckle intensity assumes form

$$R_I(\Delta x,\Delta y) = \langle I\rangle^2 [1+|\mu_A(\Delta x,\Delta y)|^2] = \langle I\rangle^2 \left[1+\left| \frac{\int_{-\infty}^{\infty}\int |P(\xi,\eta)|^2 \exp\left[i\frac{2\pi}{\lambda z}(\xi\,\Delta x+\eta\,\Delta y)\right] d\xi\, d\eta}{\int_{-\infty}^{\infty}\int |P(\xi,\eta)|^2\, d\xi\, d\eta}\right|^2\right] . \tag{2.81}$$

For the special case of a uniform and square scattering spot with dimensions $L \times L$ meters, we have

$$|P(\xi,\eta)|^2 = \text{rect}\frac{\xi}{L}\,\text{rect}\frac{\eta}{L}, \tag{2.82}$$

where $\text{rect}\,x = 1$ for $|x| \leq \frac{1}{2}$, zero otherwise. The autocorrelation function of intensity is then given by

$$R_I(\Delta x,\Delta y) = \langle I\rangle^2\left[1+\text{sinc}^2\frac{L\Delta x}{\lambda z}\,\text{sinc}^2\frac{L\Delta y}{\lambda z}\right], \tag{2.83}$$

and is illustrated in Fig. 2.15a. The "average width" of a speckle can reasonably be taken to be the value of Δx where $\text{sinc}^2(L\Delta x/\lambda z)$ first falls to zero. Denoting this distance by δx, we have

$$\delta x = \frac{\lambda z}{L}. \tag{2.84}$$

Another quantity of considerable interest is the *power spectral density* of the speckle intensity distribution $I(x,y)$, which was first

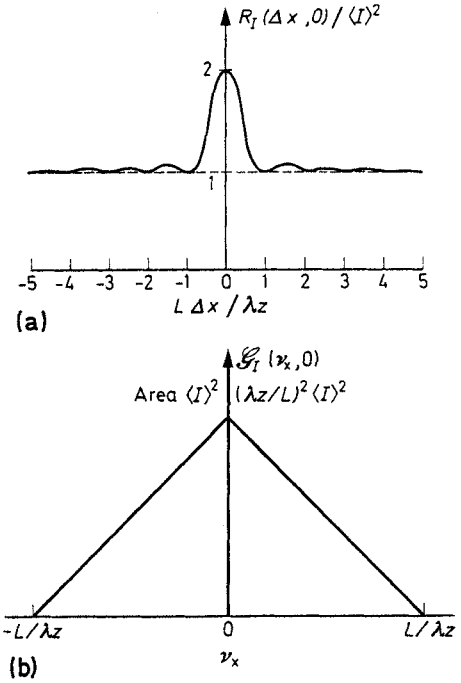

Fig. 2.15a and b. Form of the (a) autocorrelation function and (b) power spectral density of speckle produced by a square scattering spot

calculated by GOLDFISCHER [2.39]. As implied by the Wiener-Khintchine theorem [Ref. 2.11, p. 141], the power spectral density $\mathscr{G}_I(\nu_X, \nu_Y)$ of $I(x,y)$ is given by the Fourier transform of the autocorrelation function $R_I(\Delta x, \Delta y)$. Applying a Fourier transformation to (2.81), we obtain

$$\mathscr{G}_I(\nu_X, \nu_Y) = \langle I \rangle^2 \left\{ \delta(\nu_X, \nu_Y) + \frac{\int\int_{-\infty}^{\infty} |P(\xi,\eta)|^2 \, |P(\xi - \lambda z \nu_X, \eta - \lambda z \nu_Y)|^2 \, d\xi \, d\eta}{\left[\int\int_{-\infty}^{\infty} |P(\xi,\eta)|^2 \, d\xi \, d\eta \right]^2} \right\}. \tag{2.85}$$

Stated in words, the power spectral density of the speckle pattern consists of a δ-function component at zero frequency ($\nu_X = \nu_Y = 0$) plus a component extended over frequency and having the shape of the normalized autocorrelation function of the intensity distribution incident on the scattering spot. Half of the power is contained in the zero-frequency component and half appears in the extended component.

For the particular case of a uniform and square scattering spot, the power spectral density is of the form

$$\mathscr{G}_I(\nu_X, \nu_Y) = \langle I \rangle^2 \left[\delta(\nu_X, \nu_Y) + \left(\frac{\lambda z}{L} \right)^2 \Lambda\left(\frac{\lambda z}{L} \nu_X \right) \Lambda\left(\frac{\lambda z}{L} \nu_Y \right) \right] \tag{2.86}$$

where $\Lambda(x) = 1 - |x|$ for $|x| \leq 1$, zero otherwise. This distribution of power is illustrated in Fig. 2.15b. Note the speckle pattern contains no frequency components higher than $L/\lambda z$ cycles/m in the ν_X- and ν_Y-directions.

For the results of an experimental investigation of the autocorrelation function and power spectral density of a speckle pattern, see [2.21].

2.5.2 Autocorrelation Function and Power Spectral Density — Imaging Geometry

If the speckle pattern of interest occurs in an imaging geometry, such as illustrated in Fig. 2.16, rather than the free space geometry considered earlier, then some modifications must be made in the previous results. An analysis of this case has been published by LOWENTHAL and ARSENAULT [2.40]. Our analysis follows more closely that of ZERNIKE [2.41] for the analogous problem of calculating the mutual intensity in the image of an incoherent object.

Let the object of concern be uniformly reflective (or transmissive), and let the extent of the illuminated region be broad compared with the resolution cell associated with the lens used. Then, provided the

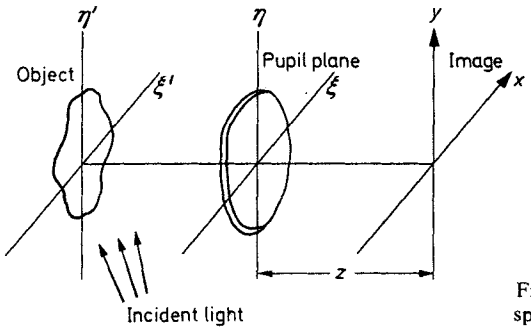

Fig. 2.16 Imaging geometry for speckle formation

object illumination is uniform, the size of the speckles incident on the lens pupil is extremely small compared with the diameter of that pupil. It follows that, to a good approximation, the mutual intensity of the fields *in the lens pupil* is given by (2.77), where now the coordinate system (ξ,η) lies in the pupil plane (see Fig. 2.16) and $P(\xi,\eta)$ is the (possibly complex-valued) pupil function of the lens. In effect, we treat the pupil plane as a uniformly bright rough surface and calculate the autocorrelation function and power spectral density of the speckle that results in the image plane.

Since only free-space propagation is involved as the light passes from the pupil plane to the image plane, the results of the previous section can now be directly applied, provided the new interpretation of $P(\xi,\eta)$ is used. In accord with (2.81), the autocorrelation function of the speckle intensity pattern consists of a constant term plus the squared modulus of the normalized Fourier transform of the *intensity* transmittance $|P(\xi,\eta)|^2$ of the lens pupil. Note that the autocorrelation function is accordingly independent of any aberrations that may be associated with the imaging system, for such aberrations affect only the phase of $P(\xi,\eta)$.

Similarly, in accord with (2.85), the power spectral density of the speckle pattern in the image plane consists of a δ-function component at zero spatial frequency, plus an extended component that takes the shape of the autocorrelation function of the intensity transmittance $|P(\xi,\eta)|^2$ of the lens pupil. For the usual case of a circular lens pupil of diameter D, the autocorrelation function and power spectral density of the image-plane speckle are

$$R_I(r)=\langle I\rangle^2\left[1+\left|2\frac{J_1\left(\frac{\pi Dr}{\lambda z}\right)}{\frac{\pi Dr}{\lambda z}}\right|^2\right] \tag{2.87}$$

where $r=[(\Delta x)^2+(\Delta y)^2]^{1/2}$, and

$$\mathscr{G}_I(\rho)=\langle I\rangle^2\left\{\delta(v_X,v_Y)+\left(\frac{\lambda z}{D}\right)^2\cdot\frac{4}{\pi}\left[\cos^{-1}\left(\frac{\lambda z}{D}\rho\right)-\frac{\lambda z}{D}\rho\sqrt{1-\left(\frac{\lambda z}{D}\rho\right)^2}\right]\right\} \tag{2.88}$$

for $\rho\leq D/\lambda z$, and zero otherwise, where $\rho=(v_X^2+v_Y^2)^{1/2}$.

2.5.3 Second-Order Probability Density Function of Intensity and Phase

While the autocorrelation function and the power spectral density are important second-order statistical properties of a speckle pattern, they do not, in themselves, provide a complete second-order statistical description of the random phenomenon. Accordingly, in this subsection we derive the second-order probability density functions of intensity and phase.

Let $A_1=A_1^{(r)}+iA_1^{(i)}$ and $A_2=A_2^{(r)}+iA_2^{(i)}$ represent samples of the complex field at points (x_1,y_1) and (x_2,y_2) in a speckle pattern. To specify the joint probability density function of A_1 and A_2, it is necessary to state the fourth-order joint probability density function of the real-valued variables $A_1^{(r)}, A_1^{(i)}, A_2^{(r)}$ and $A_2^{(i)}$. Due to the circular complex Gaussian statistics of A_1 and A_2, this joint density function takes the form (c.f. [Ref. 2.11, p. 399] and [Ref. 2.12, p. 162])

$$p(A_1^{(r)},A_1^{(i)},A_2^{(r)},A_2^{(i)})=\frac{\exp\left[-\dfrac{|A_1|^2+|A_2|^2-\mu_A A_1 A_2^*-\mu_A^* A_1^* A_2}{2\sigma^2(1-|\mu_A|^2)}\right]}{4\pi^2\sigma^4(1-|\mu_A|^2)} \tag{2.89}$$

where μ_A is the complex coherence factor of (2.79), and it has been assumed that $\langle|A_1|^2\rangle=\langle|A_2|^2\rangle=2\sigma^2$.

We wish to find the joint statistics of I_1, I_2, θ_1 and θ_2, i.e., the intensities and phases of the light at the two points in question. The corresponding transformation of variables,

$$\begin{aligned} A_1^{(r)}&=\sqrt{I_1}\cos\theta_1, \quad & A_2^{(r)}&=\sqrt{I_2}\cos\theta_2 \\ A_1^{(i)}&=\sqrt{I_1}\sin\theta_1, \quad & A_2^{(i)}&=\sqrt{I_2}\sin\theta_2, \end{aligned} \tag{2.90}$$

is readily found to have a Jacobian of 1/4. Noting that $\mu_A = |\mu_A| \exp(i\psi)$, we obtain

$$p_{I,\theta}(I_1, I_2, \theta_1, \theta_2) = \frac{\exp\left[- \dfrac{I_1 + I_2 - 2\sqrt{I_1 I_2}|\mu_A| \cos(\theta_1 - \theta_2 + \psi)}{2\sigma^2(1 - |\mu_A|^2)} \right]}{16\pi^2 \sigma^4 (1 - |\mu_A|^2)}. \tag{2.91}$$

To find the joint density function of I_1 and I_2 alone, we integrate (2.91) over θ_1 and θ_2,

$$p_I(I_1, I_2) = \int_{-\pi}^{+\pi} \int p_{I,\theta}(I_1, I_2, \theta_1, \theta_2) d\theta_1 \, d\theta_2 \,. \tag{2.92}$$

The integrand is periodic in both θ_1 and θ_2; as a consequence, it is possible to first hold θ_1 fixed and integrate over one period of $\gamma = \theta_1 - \theta_2 + \psi$, then integrate over θ_1. Thus we have

$$\begin{aligned} p_I(I_1, I_2) &= \int_{-\pi}^{\pi} d\theta_1 \int_{-\pi}^{\pi} d\gamma \, p_{I,\theta}(I_1, I_2, \theta_1, \theta_2) \\ &= \frac{\exp\left[- \dfrac{I_1 + I_2}{2\sigma^2(1 - |\mu_A|^2)} \right]}{4\sigma^4(1 - |\mu_A|^2)} \cdot \frac{1}{2\pi} \int_{-\pi}^{\pi} \exp\left[- \frac{\sqrt{I_1 I_2}|\mu_A| \cos\gamma}{\sigma^2(1 - |\mu_A|^2)} \right] d\gamma. \end{aligned} \tag{2.93}$$

Using the integral identity of (2.58), we obtain the final result

$$p_I(I_1, I_2) = \frac{\exp\left[- \dfrac{I_1 + I_2}{\langle I \rangle (1 - |\mu_A|^2)} \right]}{\langle I \rangle^2 (1 - |\mu_A|^2)} I_0\left(\frac{2\sqrt{I_1 I_2}|\mu_A|}{\langle I \rangle (1 - |\mu_A|^2)} \right), \tag{2.94}$$

where again $I_0(\cdots)$ is a modified Bessel function of the first kind, zero order.

The shape of the joint density function $p_I(I_1, I_2)$ in the (I_1, I_2) plane depends markedly on the value of the modulus of the complex coherence factor, $|\mu_A|$. Here it suffices to note two limiting cases. When the complex coherence factor goes to zero (as happens, for example, when the two measurement points are far apart), it is easily seen that

$$p_I(I_1, I_2) \doteq \left(\frac{1}{\langle I \rangle} e^{-\frac{I_2}{\langle I \rangle}} \right) \left(\frac{1}{\langle I \rangle} e^{-\frac{I_1}{\langle I \rangle}} \right) = p_I(I_1) p_I(I_2) \tag{2.95}$$

and the two intensity values are thus statistically independent. On the other hand, if the two measurement points approach each other arbitrarily closely, $|\mu_A| \to 1$, and the proper limiting argument shows that

$$p_I(I_1, I_2) \doteq p_I(I_1)\delta(I_2 - I_1). \tag{2.96}$$

In some cases it is of interest to know the conditional probability density function of I_2, given that the value of intensity is known to be I_1 at point (x_1, y_1). This density function is easily found as follows

$$p_I(I_2 | I_1) = \frac{p_I(I_1, I_2)}{p_I(I_1)} = \frac{\exp\left[-\dfrac{|\mu_A|^2 I_1 + I_2}{\langle I \rangle (1 - |\mu_A|^2)}\right]}{\langle I \rangle (1 - |\mu_A|^2)} I_0\left(\frac{2\sqrt{I_1 I_2}|\mu_A|}{\langle I \rangle (1 - |\mu_A|^2)}\right). \tag{2.97}$$

Fig. 2.17a shows plots of this density function for various values of $|\mu_A|$ with $I_1 = 1$ and $2\sigma^2 = 1$. Note that as the correlation $|\mu_A|$ increases, the probable values of I_2 begin to cluster about the known value of I_1. Fig. 2.17b exhibits plots of $p_I(I_2 | I_1)$ for a fixed correlation coefficient $|\mu_A| = 2/\pi$ and different values of the known intensity I_1 (again, $2\sigma^2 = 1$). Note that as the known value of I_1 increases, the probable values of I_2 likewise increase, due to the correlation between them. A comparison (2.59) and (2.97) demonstrates the interesting fact that the conditional density function for I_2 is identical with the density function for the sum of a coherent background and a speckle pattern, provided the associations

$$\begin{aligned} \langle I_N \rangle &= \langle I \rangle (1 - |\mu_A|^2) \\ I_S &= |\mu_A|^2 I_1 \end{aligned} \tag{2.98}$$

are made.

As a final point regarding the intensities, we note that the joint moments of I_1 and I_2 can be expressed in the form [Ref. 2.11, p. 402]

$$\langle I_1^n I_2^m \rangle = \langle I \rangle^{n+m} n! m! \, {}_2F_1(-n, -m; 1; |\mu_A|^2) \tag{2.99}$$

where ${}_2F_1$ is a Gaussian hypergeometric function and we have assumed that $\langle I_1 \rangle = \langle I_2 \rangle = \langle I \rangle$. For the particular case $n = m = 1$, we obtain

$$\langle I_1 I_2 \rangle = \langle I \rangle^2 (1 + |\mu_A|^2) \tag{2.100}$$

in accord with (2.74).

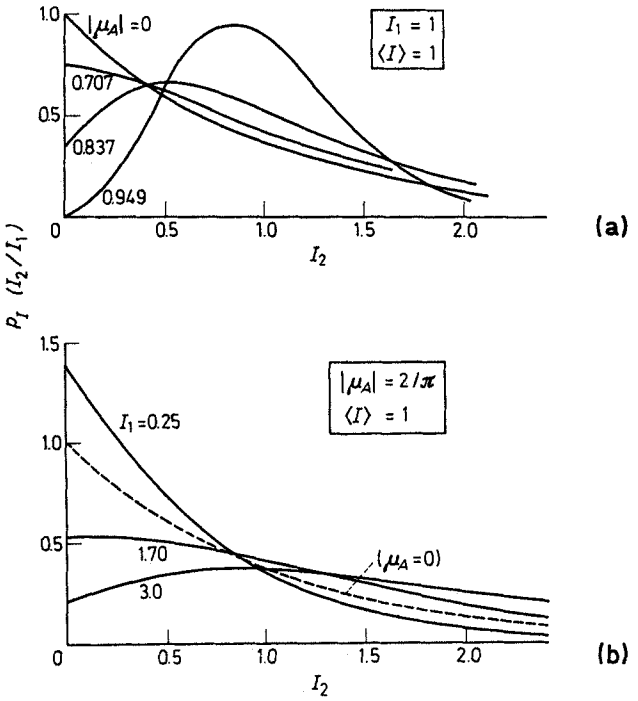

Fig. 2.17a and b. Conditional probability density function $p_I(I_a|I_1)$ vs. I_2, (a) for various values of $|\mu_A|$ with $I_1 = 1, \langle I \rangle = 1$, and (b) for various values of I_1, with $|\mu_A| = 2/\pi$ and $\langle I \rangle = 1$, (Courtesy of R.C. SMITH)

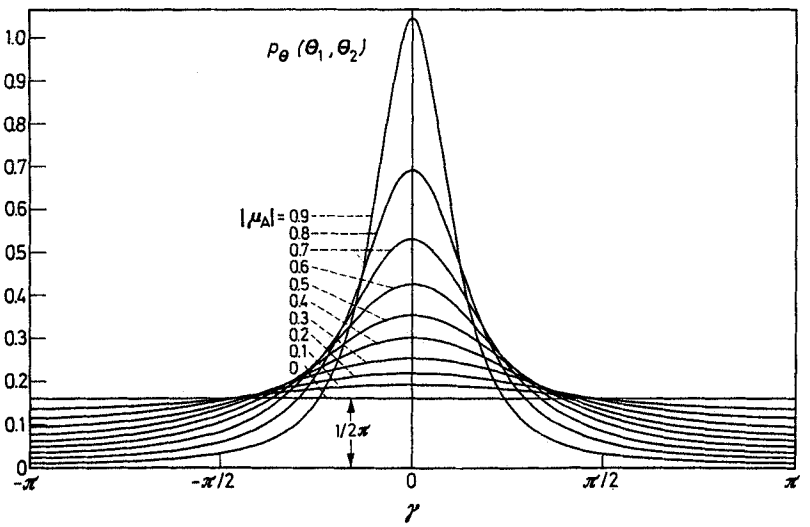

Fig. 2.18. Joint probability density $p_\theta(\theta_1, \theta_2)$ vs. $\gamma = \theta_2 - \theta_1 + \psi$ for various values of $|\mu_A|$ (after MIDDLETON [Ref. 2.11, p. 406])

We close this subsection with a brief discussion of the joint probability density function of the phases θ_1 and θ_2. In this case, the fourth-order probability density function $p_{I,\theta}(I_1, I_2, \theta_1, \theta_2)$ must be integrated with respect to the intensities I_1 and I_2. The integration is a difficult one and will not be detailed here (see [Ref. 2.11, p. 404] and [Ref. 2.12, p. 163]), but the result is

$$p_\theta(\theta_1, \theta_2) = \frac{1-|\mu_A|^2}{4\pi^2}(1-\beta^2)^{3/2}\left(\beta \sin^{-1}\beta + \frac{\pi\beta}{2} + \sqrt{1-\beta^2}\right) \quad (2.101)$$

where $\beta = |\mu_A| \cos(\theta_2 - \theta_1 + \psi)$ and both θ_1 and θ_2 must lie in the interval $(-\pi, \pi)$. Figure 2.18 shows plots of $p_\theta(\theta_1, \theta_2)$ vs. the variable $\gamma = \theta_2 - \theta_1 + \psi$ for various values of $|\mu_A|$. As the correlation $|\mu_A|$ increases, the probability density becomes more and more concentrated about small values of phase difference, indicating that the phases are more and more likely to be close together (assuming $\psi = 0$).

2.6 First-Order Statistics of Integrated and Blurred Speckle Patterns

In the experimental measurement of the intensity in a speckle pattern, the detector aperture must of necessity be of finite size. Hence the measured intensity is always a somewhat smoothed or integrated version of the ideal point-intensity, and the statistics of the measured speckle will be somewhat different than the ideal statistics developed in Subsection 2.2.3. A similar effect is observed if the speckle pattern is for some reason blurred, as could be the case, for example, if the scattering surface were in motion during the measurement. Accordingly, we consider in this section the first-order statistics of the intensity of integrated and blurred speckle patterns. Attention is limited primarily to polarized speckle patterns. A general approach for the case of partially polarized speckle patterns is briefly discussed in Subsection 2.6.4.

2.6.1 Mean and Variance of Integrated and Blurred Speckle

If a speckle pattern with intensity distribution $I(x,y)$ falls upon a detector with extended aperture, the measured intensity can be expressed in the form

$$I_0 = \frac{1}{S}\int_{-\infty}^{\infty}\int \mathscr{P}(x,y) I(x,y)\, dx\, dy\,, \quad (2.102)$$

where $\mathscr{S}(x,y)$ is a real and positive weighting function and $S = \int_{-\infty}^{\infty}\int \mathscr{S}(x,y)\,dx\,dy$. In the event that the detector has uniform response over a finite aperture, the weighting function $\mathscr{S}(x,y)$ has the simple form

$$\mathscr{S}(x,y) = \begin{cases} 1 & \text{in the aperture} \\ 0 & \text{outside the aperture,} \end{cases} \tag{2.103}$$

and S is the area of that aperture. Similarly, if we consider the intensity measured by an ideal point detector when the speckle pattern is in motion, the measured intensity can also be expressed by (2.102), where the weighting function $\mathscr{S}(x,y)$ now depends on the details of the form of motion and the measurement time. When the speckle pattern moves along the y-axis with constant velocity v, the weighting function takes the special form

$$\mathscr{S}(x,y) = \delta(x)\,\text{rect}\,\frac{y}{vT} \tag{2.104}$$

where T is the integration time.

Our goal in this subsection is to find expressions for the mean and variance of the measured intensity. The mean of I_0 is readily found from (2.102). Interchange of orders of integration and averaging yields

$$\langle I_0 \rangle = \frac{1}{S}\int_{-\infty}^{\infty}\int \mathscr{S}(x,y)\langle I\rangle\,dx\,dy = \langle I\rangle \tag{2.105}$$

where it has been assumed, in accord with the model of Subsection 2.5.1, that the mean $\langle I\rangle$ is independent of coordinates (x,y). Thus the mean of the measured intensity is exactly equal to the true mean of the speckle pattern.

Turning attention to the variance of I_0, we first calculate the second moment $\langle I_0^2\rangle$ as follows

$$\langle I_0^2\rangle = \frac{1}{S^2}\int_{-\infty}^{\infty}\int\int_{-\infty}^{\infty}\int \mathscr{S}(x_1,y_1)\mathscr{S}(x_2,y_2)\langle I(x_1,y_1)I(x_2,y_2)\rangle\,dx_1\,dy_1\,dx_2\,dy_2\,. \tag{2.106}$$

The average within the integrand is recognized to be the autocorrelation function of the speckle pattern, $R_I(x_1,y_1;x_2,y_2)$. Under the assumption that the speckle pattern has spatially stationary statistics (as is implied by the model of Subsect. 2.5.1), the autocorrelation function depends

only on the coordinate differences $\Delta x = x_1 - x_2$, $\Delta y = y_1 - y_2$, and (2.106) can be directly reduced to

$$\langle I_0^2 \rangle = \frac{1}{S^2} \int_{-\infty}^{\infty} \int R_S(\Delta x, \Delta y) R_I(\Delta x, \Delta y) d\Delta x \, d\Delta y \tag{2.107}$$

where

$$R_S(\Delta x, \Delta y) \doteq \int_{-\infty}^{\infty} \int \mathscr{S}(x_1, y_1) \mathscr{S}(x_1 - \Delta x, y_1 - \Delta y) dx_1 \, dy_1 \,. \tag{2.108}$$

At this point, the circular complex Gaussian statistics of the underlying speckle fields are invoked to write

$$R_I(\Delta x, \Delta y) = \langle I \rangle^2 [1 + |\mu_A(\Delta x, \Delta y)|^2] \tag{2.109}$$

where μ_A is again the complex coherence factor of the speckle field. The second moment of I_0 thus takes the form

$$\begin{aligned} \langle I_0^2 \rangle = & \frac{\langle I \rangle^2}{S^2} \int_{-\infty}^{\infty} \int R_S(\Delta x, \Delta y) d\Delta x \, d\Delta y \\ & + \frac{\langle I \rangle^2}{S^2} \int_{-\infty}^{\infty} \int R_S(\Delta x, \Delta y) |\mu_A(\Delta x, \Delta y)|^2 d\Delta x \, d\Delta y \,. \end{aligned} \tag{2.110}$$

The first term reduces to $\langle I \rangle^2$, and we see that the variance of the measured intensity is given by

$$\sigma_{I_0}^2 = \frac{\langle I \rangle^2}{S^2} \int_{-\infty}^{\infty} \int R_S(\Delta x, \Delta y) |\mu_A(\Delta x, \Delta y)|^2 d\Delta x \, d\Delta y \,. \tag{2.111}$$

A quantity of considerable experimental interest is what might be called the "rms signal-to-noise ratio" (or, consistent with our previous usage, the reciprocal of the contrast) of the measurement I_0,

$$\left(\frac{S}{N} \right)_{\text{rms}} \doteq \frac{\langle I_0 \rangle}{\sigma_{I_0}} \,. \tag{2.112}$$

Using the results of (2.105) and (2.111), we find that

$$\left(\frac{S}{N} \right)_{\text{rms}} = [\mathscr{M}]^{1/2} \tag{2.113}$$

where

$$\mathscr{M} \doteq \left[\frac{1}{S^2}\int\int_{-\infty}^{\infty} R_S(\Delta x, \Delta y)|\mu_A(\Delta x, \Delta y)|^2\, d\Delta x\, d\Delta y\right]^{-1}. \tag{2.114}$$

The parameter $\mathscr{M}$ will be found to be of fundamental importance in determining the first-order statistics of I_0. Accordingly, some discussion of its general behavior is in order. Physical insight is best obtained by considering two limiting cases. First, suppose that the area of the measurement aperture is much greater than the correlation area of the speckle pattern, in which case

$$\mathscr{M} \cong \left[\frac{R_S(0,0)}{S^2}\int\int_{-\infty}^{\infty} |\mu_A(\Delta x, \Delta y)|^2\, d\Delta x\, d\Delta y\right]^{-1}. \tag{2.115}$$

The integral has the dimensions of area, and can reasonably be called the correlation area S_c of the speckle pattern,

$$S_c = \int\int_{-\infty}^{\infty} |\mu_A(\Delta x, \Delta y)|^2\, d\Delta x\, d\Delta y\,. \tag{2.116}$$

The constant factor preceding the integral has the dimensions of (area)$^{-1}$, and its reciprocal can reasonably be called the effective measurement area, S_m, defined by

$$S_m \doteq \frac{S^2}{\int\int_{-\infty}^{\infty} \mathscr{S}^2(\Delta x, \Delta y)\, d\Delta x\, d\Delta y}. \tag{2.117}$$

In the case of a simple measurement aperture, with $\mathscr{S}$ equal to unity or zero, S_m is equal to S, the physical area of the aperture. In terms of the areas S_m and S_c, we find that

$$\mathscr{M} \cong \frac{S_m}{S_c}, \quad (S_m \gg S_c), \tag{2.118}$$

and thus $\mathscr{M}$ can be interpreted as the number of speckle correlation cells within the measurement aperture.

For the opposite extreme of an aperture very small compared with the correlation area of the speckle, we have $|\mu_A|^2 \cong 1$, and

$$\mathscr{M} \cong \left[\frac{1}{S^2}\int\int_{-\infty}^{\infty} R_S(\Delta x, \Delta y)\, d\Delta x\, d\Delta y\right]^{-1} = 1, \quad (S_m \ll S_c). \tag{2.119}$$

This result may be interpreted as indicating that, as the measurement aperture shrinks, the number of correlation cells influencing the measured intensity I_0 asymptotically approaches unity. Values of less than unity are not possible, for the experimental results are always influenced by the intensity in at least one correlation cell.

An exact expression for $\mathscr{M}$ valid for all aperture sizes requires knowledge of the complex coherence factor μ_A and the aperture function $\mathscr{S}$. For a square aperture of $L \times L$ square meters, and a Gaussian shaped complex coherence factor (corresponding to a Gaussian shaped intensity pattern incident on the scattering spot), we have

$$\mu_A(\Delta x, \Delta y) = \exp\left\{ -\frac{\pi}{2S_c}\left[(\Delta x)^2 + (\Delta y)^2\right]\right\} \tag{2.120}$$

and an exact expression for $\mathscr{M}$ can be shown to be

$$\mathscr{M} = \left\{ \sqrt{\frac{S_c}{S_m}}\,\mathrm{erf}\left(\sqrt{\frac{\pi S_m}{S_c}}\right) - \left(\frac{S_c}{\pi S_m}\right)\left[1 - \exp\left(-\frac{\pi S_m}{S_c}\right)\right]\right\}^{-2} \tag{2.121}$$

where

$$\mathrm{erf}(x) \doteq \frac{2}{\sqrt{\pi}} \int_0^x e^{-z^2} dz \tag{2.122}$$

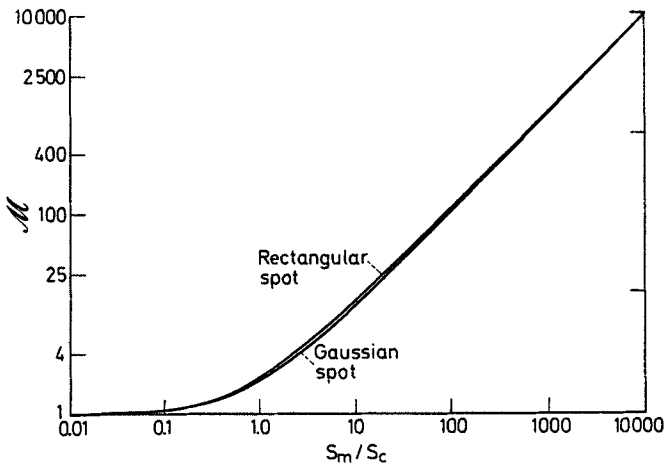

Fig. 2.19. Number $\mathscr{M}$ of correlation cells vs. S_m/S_c for a scattering spot with a Gaussian intensity profile and a square detector

and $S_m = L^2$. For the case of a square scattering spot, we have

$$\mu_A(\Delta x, \Delta y) = \operatorname{sinc} \frac{\Delta x}{\sqrt{S_c}} \operatorname{sinc} \frac{\Delta y}{\sqrt{S_c}} \tag{2.123}$$

and the expression for $\mathscr{M}$ becomes

$$\mathscr{M} = \left[\frac{1}{\sqrt{S_m}} \int_{-\infty}^{\infty} \Lambda\left(\frac{\Delta x}{\sqrt{S_m}} \right) \operatorname{sinc}^2 \frac{\Delta x}{\sqrt{S_c}} \, d\Delta x \right]^{-2}. \tag{2.124}$$

Figure 2.19 shows a plot of $\mathscr{M}$ vs. S_m/S_c for both Gaussian and square scattering spots, with a square measurement aperture assumed in both cases. Values of $\mathscr{M}$ for the square scattering spot have been obtained by numerical integration of (2.124) (c.f. [Ref. 2.17, Fig. 4]).

2.6.2 Approximate Form for Probability Density Function of Integrated Speckle

In many applications, more than just the rms signal-to-noise ratio of an integrated speckle pattern is required. Most often, the first-order probability density function of the integrated intensity I_0 may be desired. In this subsection, we derive an approximate form for this density function, following the approach of RICE [2.42], MANDEL [2.10] and GOODMAN [2.17]. As a first approximation, the smoothly varying speckle intensity $I(x,y)$ may be replaced on the measurement area by a two-dimensional "box-car" function, as illustrated in Fig. 2.20. The measurement area is divided into m equal and identically shaped sub-areas. Within each sub-area, the approximation is made that $I(x,y)$ is constant; outside of a given sub-area, the approximate intensity distribution jumps to a new constant value, assumed statistically independent of the constant values in all other sub-areas. The probability density function of the box-car function in any one sub-area is taken to be the same as the first-order density function of $I(x,y)$, i.e., a negative-exponential density for polarized speckle. The mean intensity in all sub-areas is taken to be the same.

The integrated intensity may be approximated as the normalized volume under the box-car

$$I_0 = \frac{1}{S} \int_{-\infty}^{\infty} \mathscr{S}(x,y) I(x,y) \, dx \, dy = \frac{1}{S} \sum_{k=1}^{m} \mathscr{S}_k I_k \tag{2.125}$$

where $\mathscr{S}_k$ is the volume under $\mathscr{S}(x,y)$ in the kth box-car cell and I_k is the constant intensity assumed in that cell.

The characteristic function of each I_k is taken to be that of polarized speckle at a single point,

$$M_k(iv) = \frac{1}{1-iv\langle I\rangle}. \tag{2.126}$$

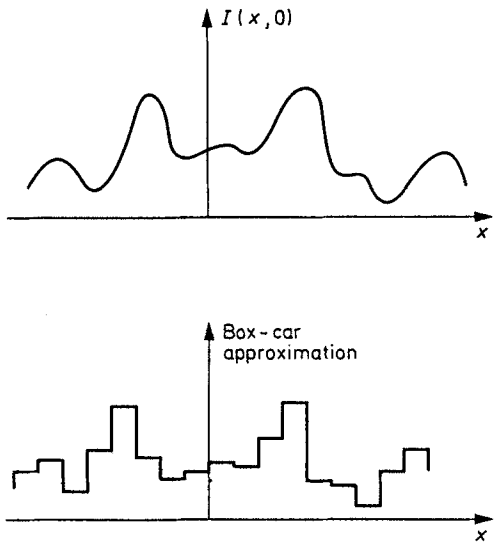

Fig. 2.20. Box-car approximation to $I(x,y)$, cross section with $y=0$

It follows that the characteristic function of the integrated speckle is given approximately by

$$M_{I_0}(iv) \cong \prod_{k=1}^{m} \frac{1}{1-iv\dfrac{\mathscr{S}_k}{S}\langle I\rangle}. \tag{2.127}$$

The form of the approximate density function for I_0 depends on whether the constants $\mathscr{S}_k\langle I\rangle/S$ are distinct or if some or all of these constants are equal. At this point we specialize to the case of a simple detection aperture with $\mathscr{S}=0$ or 1. In this case,

$$\frac{\mathscr{S}_k}{S} = \frac{1}{m} \quad \text{all} \quad k, \tag{2.128}$$

and the characteristic function becomes

$$M_{I_0}(iv) \cong \left[\frac{1}{1 - iv\dfrac{\langle I\rangle}{m}}\right]^m. \tag{2.129}$$

The corresponding probability density function is the gamma density function,

$$p_{I_0}(I_0) \cong \begin{cases} \dfrac{\left(\dfrac{m}{\langle I\rangle}\right)^m I_0^{m-1} \exp\left(-m\dfrac{I_0}{\langle I\rangle}\right)}{\Gamma(m)} & I \geq 0 \\ 0 & \text{otherwise,} \end{cases} \tag{2.130}$$

where $\Gamma(m)$ is a gamma function of argument m.

The gamma density function has two parameters, m and $\langle I\rangle$, which we are free to choose in a manner which will closely match the approximate density function to the true density function. The simplest approach is to choose $\langle I\rangle$ and m to match the first two moments of the gamma density function to the exact first and second moments, which are known from Subsection 2.6.1. This match is accomplished if m is chosen to equal the parameter $\mathscr{M}$ of (2.114) and if $\langle I\rangle$ is chosen equal to the true mean of the speckle intensity $I(x,y)$. Thus the approximate density function is of the form

$$p_{I_0}(I_0) \cong \frac{\left(\dfrac{\mathscr{M}}{\langle I\rangle}\right)^{\mathscr{M}} I_0^{\mathscr{M}-1} \exp\left(-\mathscr{M}\dfrac{I_0}{\langle I\rangle}\right)}{\Gamma(\mathscr{M})} \tag{2.131}$$

for $I_0 \geq 0$.

Note that the parameter $\mathscr{M}$ need not be an integer, and so the quasi-physical picture of the box-car approximation partially breaks down. However, we can abandon this quasi-physical picture, and simply regard (2.131) as a mathematical form which approximates the true density function. It should further be noted that, while choosing the parameters of the gamma density to match the first two moments with exact values seems reasonable, there is no reason to assume that this is the best way to choose the parameters. It is, however, the simplest way, and accordingly it is usually used.

Figure 2.21 shows plots of $p_{I_0}(I_0)$ for several values of the parameter $\mathscr{M}$. Note that when $\mathscr{M} \to 1$ (i.e., the measurement aperture shrinks

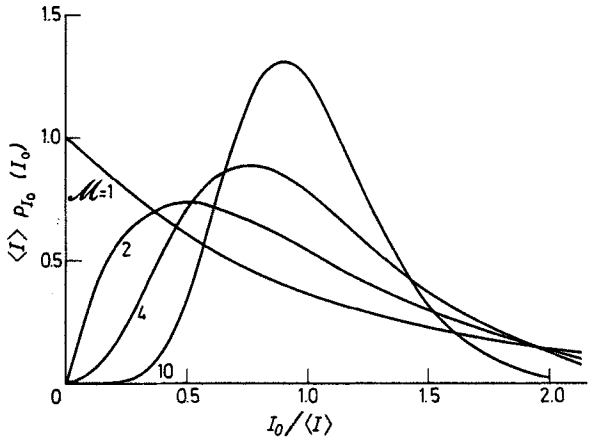

Fig. 2.21. Probability density function $p_{I_0}(I_0)$ for several values of the parameter $\mathscr{M}$

towards zero size), the density function approaches the negative exponential function valid for speckle intensity at a point. As $\mathscr{M} \to \infty$, the gamma density function can be shown to approach a Gaussian density function. By virtue of the central limit theorem, this is indeed the exact density function in the limit of $\mathscr{M} \to \infty$. Thus the gamma density function is highly accurate for $\mathscr{M}$ near zero and $\mathscr{M}$ very large. For intermediate values of $\mathscr{M}$, we expect the approximate density function to depart from the true density somewhat.

2.6.3 Exact Probability Density Function of Integrated Speckle

By means of a mathematical formalism known as the Karhunen-Loève expansion ([Ref. 2.12, p. 96] and [Ref. 2.11, p. 380]), it is possible to arrive at an exact expression for the probability density function of the integrated speckle intensity I_0. This formalism was first used in the speckle context by CONDIE [2.19], who calculated the cumulants of the exact distribution and compared them with the cumulants of the gamma distribution. DAINTY [2.43] and BARAKAT [2.27] applied the same method to find general expressions for the probability density function of I_0. BARAKAT [2.27] plotted exact probability density functions for the case of a slit aperture and a Gaussian correlation function μ_A (implying a Gaussian brightness distribution across the scattering spot). SCRIBOT [2.44] has found exact probability density functions for the case of a slit aperture and a sinc autocorrelation function (or a rectangular scattering spot), and has compared the exact and approximate density functions.

To find the exact form of the probability density function of I_0, we begin by expanding the speckle fields across the measurement aperture in an orthonormal series,

$$A(x,y) = \frac{1}{\sqrt{S}} \sum_{n=0}^{\infty} b_n \phi_n(x,y), \quad (x,y) \text{ in } \Sigma, \tag{2.132}$$

where Σ refers to the region of the (x,y) plane occupied by the aperture (area S),

$$\iint_{\Sigma} \phi_m^*(x,y)\,\phi_n(x,y)\,dx\,dy = \begin{cases} 1 & n=m \\ 0 & n \neq m, \end{cases} \tag{2.133}$$

and

$$b_n = \sqrt{S} \iint_{\Sigma} A(x,y)\,\phi_n^*(x,y)\,dx\,dy. \tag{2.134}$$

Of the many possible orthogonal expansions that might satisfy these conditions, we wish to choose one that will yield uncorrelated expansion coefficients, i.e., for which

$$E[b_n b_m^*] = \begin{cases} \lambda_n & m=n \\ 0 & m \neq n. \end{cases} \tag{2.135}$$

Using (2.134) for the b's, we find the general expression for the correlation between coefficients

$$\begin{aligned} E[b_n b_m^*] &= S \iint_{\Sigma} \iint_{\Sigma} \langle A(x_1,y_1) A^*(x_2,y_2) \rangle \phi_n(x_2,y_2) \phi_m^*(x_1,y_1) dx_1\,dy_1\,dx_2\,dy_2 \\ &= \iint_{\Sigma} \left[S \iint_{\Sigma} J_A(x_1,y_1;x_2,y_2) \phi_n(x_2,y_2)\,dx_2\,dy_2 \right] \phi_m^*(x_1,y_1)\,dx_1\,dy_1. \end{aligned} \tag{2.136}$$

The constraint (2.135) can now be seen to be satisfied provided

$$S \iint_{\Sigma} J_A(x_1,y_1;x_2,y_2) \phi_n(x_2,y_2)\,dx_2\,dy_2 = \lambda_n \phi_n(x_1,y_1). \tag{2.137}$$

Thus it is necessary to choose the orthonormal functions to be eigenfunctions of the integral equation (2.137); the constants λ_n are the corresponding eigenvalues. Since the mutual intensity J_A has Hermitian symmetry and is positive definite, both λ_n and ϕ_n can be shown to be real-valued.

The integrated intensity of interest can be expressed in the form

$$I_0 = \frac{1}{S} \iint_{\Sigma} A(x,y) A^*(x,y) dx\, dy . \tag{2.138}$$

Using the expansion (2.132) and the orthogonality condition (2.133), we obtain

$$I_0 = \sum_{n=0}^{\infty} |b_n|^2 . \tag{2.139}$$

Now it follows from (2.134) and the real-valued character of the ϕ_n's that the random variables are zero mean, circular complex Gaussian random variables. Furthermore, by (2.135) they are uncorrelated and therefore independent, and have variance $\lambda_n/2$ for their real and imaginary parts. Accordingly, the characteristic function of I_0 is given exactly by

$$M_{I_0}(iv) = \prod_{n=0}^{\infty} (1 - iv\lambda_n)^{-1} . \tag{2.140}$$

If the λ_n are distinct, the corresponding probability density function is

$$p_{I_0}(I_0) = \sum_{n=0}^{\infty} \frac{d_n}{\lambda_n} \exp(-I_0/\lambda_n) \tag{2.141}$$

for $I_0 \geq 0$, where

$$d_n = \prod_{\substack{m=0 \\ m \neq n}}^{\infty} \left(1 - \frac{\lambda_m}{\lambda_n}\right)^{-1} . \tag{2.142}$$

Since $p_{I_0}(I_0)$ is a density function, its area must be unity, and it follows that $\sum_{n=0}^{\infty} d_n = 1$. The mean and variance of the exact density function are readily shown to be

$$\begin{aligned} \langle I_0 \rangle &= \sum_{n=0}^{\infty} d_n \lambda_n \\ \sigma_{I_0}^2 &= \sum_{n=0}^{\infty} 2 d_n \lambda_n^2 - \left(\sum_{n=0}^{\infty} d_n \lambda_n \right)^2 . \end{aligned} \tag{2.143}$$

The exact probability that the integrated intensity exceeds the threshold I_0 is given by

$$P(I_0) = \sum_{n=0}^{\infty} d_n \exp(-I_0/\lambda_n) . \tag{2.144}$$

Calculation of the eigenvalues λ_n requires solution of the integral equation (2.137) for the particular aperture Σ and the particular mutual intensity function $J_A(x_1,y_1;x_2,y_2)$ valid for the problem of interest. For the case of a slit aperture and a line scattering spot of uniform brightness, the solutions have been given by SCRIBOT [2.44]. The eigenfunctions are solutions to the integral equation

$$\int_{-1}^{+1} \frac{\sin[c(x_1-x_2)]}{\pi(x_1-x_2)} \phi_n(x_2)\,dx_2 = \lambda_n \phi_n(x_1) \tag{2.145}$$

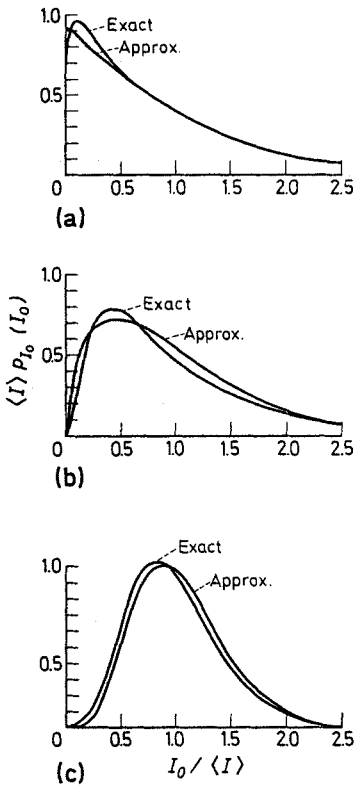

Fig. 2.22a–c. Exact density function and approximate density function $p_{I_0}(I_0)$ for (a) $c=0.5$, $\mathcal{M}=1.07$, (b) $c=2.0$, $\mathcal{M}=1.79$, and $c=8.0$, $\mathcal{M}=5.77$. (Exact curves after SCRIBOT [2.44])

and are known as the prolate spheroidal wave functions [2.45–47]. The constant c is given by

$$c = \frac{\pi}{2} \frac{L_m}{L_c} \tag{2.146}$$

where L_m is the width of the measurement aperture and L_c is the correlation width of the speckle pattern (the one-dimensional analog of the correlation area S_c of (2.116)).

Figures 2.22a, b and c show plots of the exact density function (adapted from the computed results of SCRIBOT [2.44]) and the approximate density functions from the theory of Subsection 2.6.2. The approximate density functions differ from those of SCRIBOT, due to a different method for choosing $\mathscr{M}$.

In closing, we note that it has been pointed out by CONDIE [2.19], BARAKAT [2.27] and SCRIBOT [2.44] that the approximate density function for I_0 given by the gamma density of (2.131) may be regarded as the result of assuming that all eigenvalues below index $\mathscr{M}$ are equal to a single constant, and all eigenvalues with larger indices are zero.

2.6.4 Integration of Partially Polarized Speckle Patterns

If the speckle patterns are partially polarized, rather than perfectly polarized, as assumed above, the theory must be modified. The general case can still be analyzed in principle, but the results are difficult to apply in practice.

The first step in the analysis of the partially polarized case is to find the transformation $\mathscr{L}_0$ that will diagonalize the coherency matrix. Using this transformation, the total intensity $I(x,y)$ in the speckle pattern can be expressed as the sum of two statistically independent intensities,

$$I(x,y) = I_a(x,y) + I_b(x,y), \tag{2.147}$$

where both I_a and I_b obey negative exponential statistics. From (2.53), if the degree of polarization is $\mathscr{P}$, then

$$\begin{aligned} \langle I_a \rangle &= \tfrac{1}{2}\langle I \rangle (1+\mathscr{P}) \\ \langle I_b \rangle &= \tfrac{1}{2}\langle I \rangle (1-\mathscr{P}). \end{aligned} \tag{2.148}$$

The integrated intensity I_0 is now represented in the form

$$I_0 = \frac{1}{S} \int_{-\infty}^{\infty} \int \mathscr{S}(x,y)[I_a(x,y) + I_b(x,y)]\,dx\,dy. \tag{2.149}$$

The mean of I_0 is easily shown to be $\langle I \rangle$. For the variance, we follow the procedure that led to (2.111), this time with the result

$$\sigma_{I_0}^2 = \tfrac{1}{4}\frac{\langle I\rangle^2(1+\mathscr{P})^2}{S^2}\int\int_{-\infty}^{\infty} R_S(\Delta x,\Delta y)|\mu_a(\Delta x,\Delta y)|^2\,d\Delta x\,d\Delta y + \tfrac{1}{4}\frac{\langle I\rangle^2(1-\mathscr{P})^2}{S^2}\int\int_{-\infty}^{\infty} R_S(\Delta x,\Delta y)|\mu_b(\Delta x,\Delta y)|^2\,d\Delta x\,d\Delta y\,, \tag{2.150}$$

where $\mu_a(\Delta x,\Delta y)$ and $\mu_b(\Delta x,\Delta y)$ represent the complex coherence factors for the fields that underlie I_a and I_b, respectively.

The problem now becomes complicated due to the fact that, in general, μ_a and μ_b need not be the same functions of Δx and Δy. After the transformation $\mathscr{L}_0$, which entails at most only coordinate rotations and phase retardations, the brightness distributions across the scattering object may not be the same in both polarization components. Such effects are readily observed experimentally if a diffusely reflecting three-dimensional model is examined through a polarization analyzer with axis alternately aligned parallel with and orthogonal to the polarization direction of the incident laser light.

To retain the required generality, we define two different parameters as follows

$$\mathscr{M}_a \doteq \left[\frac{1}{S^2}\int\int_{-\infty}^{\infty} R_S(\Delta x,\Delta y)|\mu_a(\Delta x,\Delta y)|^2\,d\Delta x\,d\Delta y\right]^{-1}$$
$$\mathscr{M}_b \doteq \left[\frac{1}{S^2}\int\int_{-\infty}^{\infty} R_S(\Delta x,\Delta y)|\mu_b(\Delta x,\Delta y)|^2\,d\Delta x\,d\Delta y\right]^{-1}. \tag{2.151}$$

In terms of these parameters, we find that the rms signal-to-noise ratio of the integrated speckle pattern is given by

$$\left(\frac{S}{N}\right)_{\text{rms}} = 2\left[\frac{(1+\mathscr{P})^2}{\mathscr{M}_a} + \frac{(1-\mathscr{P})^2}{\mathscr{M}_b}\right]^{-1/2}. \tag{2.152}$$

An approximate probability density function can be derived based on box-car approximations for $I_a(x,y)$ and $I_b(x,y)$. The derivation simply involves the inversion of a characteristic function which is the product of two terms similar to (2.129), one for I_a and the second for I_b. Exact solutions for $p_{I_0}(I_0)$ are also possible if Karhunen-Loève expansions are applied to both I_a and I_b. The characteristic function for I_0 is simply found as the product of two terms similar to (2.140). The probability density function is found by Fourier inversion of the characteristic function, with the results depending on two sets of eigenvalues, one

for each polarization component. Because the results depend strongly on various assumptions regarding the shape of the integrating aperture, the form of the functions μ_a and μ_b, and the degree of polarization $\mathscr{P}$, we will not pursue a more detailed analysis in this case.

2.7 Effects of Surface Structure on Monochromatic and Polarized Speckle Patterns

In the models of the previous sections, the scattering surfaces have been assumed to be so rough that the phases of the elementary scatterers are completely uniform. In addition, by use of (2.77), the correlation area of the reflected wave has been assumed to be so small as to be unresolvable by an aperture the size of our observation region. These assumptions are quite accurate in the majority of practical problems involving speckle. Nonetheless, it is still of considerable interest to understand the conditions under which the statistical properties of the surface *can* affect the measurable properties of the observed speckle.

Attention will be restricted here to monochromatic and fully polarized speckle patterns. Within these restrictions, we first consider the effect of a finite correlation area of the scattered wavefront at the rough surface on the correlation function of the observed speckle pattern. Second, we develop an approximate relationship between the correlation function of the scattered wave at the surface and the correlation function of the random surface itself. Finally, we consider some first-order statistical properties of speckle as a function of surface roughness.

Previous work on the effects of surface detail on speckle is not plentiful. The classic work on scattering of electromagnetic waves from rough surfaces [2.14] contains much that is applicable. Work directly in the context of laser speckle was reported by CRANE [2.48], who derived results that appeared to conflict with those of GOLDFISCHER [2.39] and GOODMAN [2.13, 17]. An inconsistency in the interpretation of the non-statistical portions of Crane's paper was pointed out by ARSENAULT [2.49]. An error in the interpretation of the statistical portion of Crane's paper was found by GOODMAN [2.50], who showed that Crane's results are only valid for relatively smooth surfaces. Recently, interest has developed in the relation between surface roughness and the contrast of a speckle pattern, motivated primarily by the experimental work of FUJII and ASAKURA [2.51]. PEDERSON [2.52] has published an analysis pertinent to these experiments, in which he assumed that the diffusely scattered fields obey circular complex Gaussian statistics, even for relatively smooth surfaces. This assumption appears

justified in the case of free-space formation of speckle (Fig. 2.14), but it will be shown to be incorrect for the particular experimental geometry used by FUJII and ASAKURA. Finally, mention should be made of the work of BERNY and IMBERT [2.53], who have developed an optical instrument for measuring surface roughness based on the properties of the diffuse and specular reflected fields.

2.7.1 Effect of Finite Correlation Area of the Wave at the Rough Surface

Two different geometries will be of interest to us here. One is the free-space geometry of Fig. 2.14. The second is a modification of the free-space geometry, in which a lens is inserted such that the rough surface lies approximately in the front focal of the lens, while the observation plane lies in the back focal plane. Neglecting the finite aperture of the lens, this latter geometry effectively moves the observation plane to infinity with respect to the scattering surface. We again use coordinates (ξ,η) for the plane adjacent to the scattering surface, and coordinates (x,y) for the plane of the speckle pattern. The waves are assumed perfectly polarized, with complex amplitudes $\alpha(\xi,\eta)$ and $A(x,y)$.

The general relationship between the mutual intensities J_α in the (ξ,η) plane and J_A in the (x,y) plane was derived in Subsection 2.5.1 for the free space geometry, with the result, c.f., (2.76)

$$J_A(x_1,y_1;x_2,y_2) = \frac{1}{\lambda^2 z^2}\exp\left[-i\frac{\pi}{\lambda z}\left(x_1^2-x_2^2+y_1^2-y_2^2\right)\right] \tag{2.153}$$

$$\times\int\int_{-\infty}^{\infty}\int J_\alpha(\xi_1,\eta_1;\xi_2,\eta_2)\exp\left[-i\frac{\pi}{\lambda z}\left(\xi_1^2-\xi_2^2+\eta_1^2-\eta_2^2\right)\right]$$

$$\times\exp\left[i\frac{2\pi}{\lambda z}\left(x_1\xi_1+y_1\eta_1-x_2\xi_2-y_2\eta_2\right)\right]d\xi_1\,d\eta_1\,d\xi_2\,d\eta_2.$$

For the focal-plane-to-focal-plane geometry, the quadratic phase factors of (2.75) are missing [Ref. 2.37, Chap. 5], with the result that the above equation must be modified to read

$$J_A(x_1,y_1;x_2,y_2) = \frac{1}{\lambda^2 z^2}\int\int_{-\infty}^{\infty}\int J_\alpha(\xi_1,\eta_1;\xi_2,\eta_2) \tag{2.154}$$

$$\times\exp\left[i\frac{2\pi}{\lambda z}(x_1\xi_1+y_1\eta_1-x_2\xi_2-y_2\eta_2)\right]d\xi_1\,d\eta_1\,d\xi_2\,d\eta_2,$$

where z is now the focal length of the lens. We shall work with (2.154), and then show that under certain conditions similar results can be obtained from (2.153).

To begin with, we define

$$\begin{aligned} \Delta x &\doteq x_1 - x_2 & \Delta \xi &\doteq \xi_1 - \xi_2 \\ \Delta y &\doteq y_1 - y_2 & \Delta \eta &\doteq \eta_1 - \eta_2 \end{aligned} \tag{2.155}$$

and we note that

$$x_1\xi_1 + y_1\eta_1 - x_2\xi_2 - y_2\eta_2 = x_2\Delta\xi + y_2\Delta\eta + \Delta x\xi_1 + \Delta y\eta_1 . \tag{2.156}$$

Further, we assume that the mutual intensity J_α is of the form

$$J_\alpha(\xi_1,\eta_1;\xi_2,\eta_2) = \kappa P(\xi_1,\eta_1) P^*(\xi_2,\eta_2) \mu_\alpha(\Delta\xi,\Delta\eta) \tag{2.157}$$

where μ_α is the complex coherence factor and depends only on $\Delta\xi,\Delta\eta$. In general, the structure of the incident fields, $P(\xi_1,\eta_1)$, is extremely coarse compared with width of the complex coherence factor, and hence to an excellent approximation

$$J_\alpha(\xi_1,\eta_1;\xi_2,\eta_2) \cong \kappa |P(\xi_1,\eta_1)|^2 \mu_\alpha(\Delta\xi,\Delta\eta) . \tag{2.158}$$

Substituting this expression and (2.156) in (2.154), we obtain

$$\begin{aligned} J_A(x_1,y_1;x_2,y_2) = \frac{\kappa}{\lambda^2 z^2} \int\int_{-\infty}^{\infty} |P(\xi_1,\eta_1)|^2 \exp\left[i\frac{2\pi}{\lambda z}(\Delta x\xi_1 + \Delta y\eta_1)\right] \\ \times\ d\xi_1 d\eta_1 \ \times \int\int_{-\infty}^{\infty} \mu_\alpha(\Delta\xi,\Delta\eta) \\ \times \exp\left[i\frac{2\pi}{\lambda z}(x_2\Delta\xi + y_2\Delta\eta)\right] d\Delta\xi\, d\Delta\eta . \end{aligned} \tag{2.159}$$

This result for the mutual intensity J_A is of considerable importance, for it separates the effects of the finite size of the scattering spot (the term involving $|P(\xi_1,\eta_1)|^2$) and the correlation properties of the reflected wave in the (ξ,η) plane (the term involving $\mu_\alpha(\Delta\xi,\Delta\eta)$). Since the size of the scattering spot is generally very much greater than the coherence area of the reflected wave, we see that the first Fourier transform yields a narrow function of $(\Delta x,\Delta y)$, which may be regarded as indicating the "average size" of a speckle, while the second term yields a broad function of (x_2,y_2), which may be regarded as a coarsely varying distribution of mean intensity in the (x,y) plane. Thus we conclude that, subject to the various assumptions used in the analysis, the correlation function of the wave at the scattering surface influences only the *distribution of*

average intensity over the observation plane, and has no influence over the coarseness of the granular speckle pattern. Stated in another equivalent way, the complex coherence factor $\mu_A(\Delta x, \Delta y)$ in the (x,y) plane is unaffected by the complex coherence factor $\mu_\alpha(\Delta\xi, \Delta\eta)$ in the (ξ,η) plane.

Similar conclusions can be drawn for the free-space geometry provided certain assumptions regarding the distance z are adopted (see [Ref. 2.17, App. A]). In particular, if we assume that

$$z > 2\frac{S_c}{\lambda} \quad \text{and} \quad z > 2\frac{\sqrt{S_s S_c}}{\lambda} \tag{2.160}$$

where S_c is the coherence area in the (ξ,η) plane and S_s is the area of the scattering spot, then various quadratic factors can be dropped, with the result that (2.153) becomes

$$\begin{aligned} J_A(x_1,y_1;x_2,y_2) = \frac{1}{\lambda^2 z^2} \exp\left[-i\frac{\pi}{\lambda z}(x_1^2 - x_2^2 + y_1^2 - y_2^2)\right] \\ \times \int\int_{-\infty}^{\infty} J_\alpha(\xi_1,\eta_1;\xi_2,\eta_2) \\ \times \exp\left[i\frac{2\pi}{\lambda z}(x_1\xi_1 + y_1\eta_1 - x_2\xi_2 - y_2\eta_2)\right] d\xi_1 d\eta_1 d\xi_2 d\eta_2 . \end{aligned} \tag{2.161}$$

This result differs from (2.154) for the focal-plane-to-focal-plane geometry only through the initial quadratic phase factor, which in no way influences either the coherence area in the (x,y) plane or the distribution of average intensity. Hence the conclusions drawn for the previous geometry also apply here, provided (2.160) is satisfied.

2.7.2 Relation between the Correlation Function of the Surface and the Mutual Intensity of the Reflected Wave

The results of the preceding subsection were presented in terms of the mutual intensity of the reflected wave at the rough surface. It remains to relate this mutual intensity function to the correlation function of the rough surface itself.

With reference to Fig. 2.23, the rough surface is described by a height function $h(\xi,\eta)$ that represents the departure of the surface from its mean position. The incident plane wave arrives at angle β to the normal. The height function $h(\xi,\eta)$ is assumed to be a wide-sense stationary random process, with normalized autocorrelation function $\rho_h(\Delta\xi, \Delta\eta)$.

The relation between the height function and the complex fields in the (ξ,η) plane immediately to the right of the surface is an extremely complex one if it is developed with rigor. Many complicating factors play a role, including variations of the Fresnel reflection coefficient with

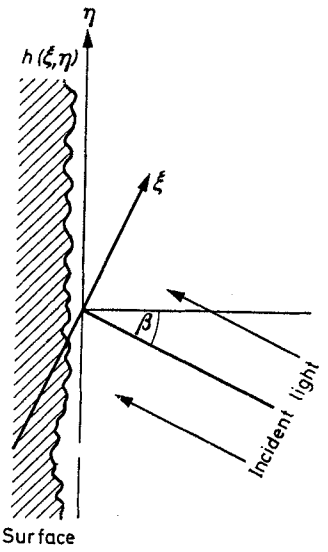

Fig. 2.23. Rough surface and the height function

slope, effects of propagation from the point of reflection to the (ξ,η) plane, multiple scattering, and shadowing. Here we adopt a simplistic relation, often used in analysis and reasonably accurate if the surface slopes are small, namely that the complex field in the (ξ,η) plane is given by

$$\alpha(\xi,\eta)=rP(\xi,\eta)\exp\left[i\frac{2\pi}{\lambda}(1+\cos\beta)h(\xi,\eta)\right] \tag{2.162}$$

where r is the average reflectivity and $P(\xi,\eta)$ is the complex field incident on the surface.

Since $h(\xi,\eta)$ is a zero mean wide-sense stationary random process, so too is the phase angle

$$\theta(\xi,\eta)=\frac{2\pi}{\lambda}(1+\cos\beta)h(\xi,\eta)\,. \tag{2.163}$$

If σ_h^2 represents the variance of h, then the variance of θ is simply

$$\sigma_\theta^2 = \left[\frac{2\pi}{\lambda}(1+\cos\beta)\right]^2 \sigma_h^2 . \tag{2.164}$$

Similary, the correlation function $R_\theta(\Delta\xi, \Delta\eta)$ of the phase is related to the normalized correlation function $\rho_h(\Delta\xi, \Delta\eta)$ of the surface heights by

$$R_\theta(\Delta\xi, \Delta\eta) = \sigma_\theta^2 \rho_h(\Delta\xi, \Delta\eta) . \tag{2.165}$$

Assuming that the structure of the incident amplitude $P(\xi, \eta)$ is coarse compared with the structure of $\theta(\xi, \eta)$, we can write the complex coherence factor of the reflected fields as

$$\mu_\alpha(\Delta\xi, \Delta\eta) = \langle \exp[i(\theta_1 - \theta_2)] \rangle \tag{2.166}$$

where $\theta_1 = \theta(\xi_1, \eta_1)$, $\theta_2 = \theta(\xi_2, \eta_2)$. This average can be expressed in terms of the second-order characteristic function of $\theta(\xi, \eta)$,

$$M_\theta(iv_1, iv_2) = \int_{-\infty}^{\infty}\int p_\theta(\theta_1, \theta_2) \exp[i(v_1\theta_1 + v_2\theta_2)]\, d\theta_1\, d\theta_2 \tag{2.167}$$

where $p_\theta(\theta_1, \theta_2)$ is the second-order probability density function of θ_1, θ_2. Thus

$$\mu_\alpha(\Delta\xi, \Delta\eta) = M_\theta(i1, -i1) . \tag{2.168}$$

Unless the second-order statistics of θ (and therefore of h) are specified, little further progress can be made.

For simplicity, the assumption is usually made that the surface height fluctuations are a Gaussian random process. In this case, the complex coherence factor μ_α takes the relatively simple form

$$\mu_\alpha(\Delta\xi, \Delta\eta) = \exp\{-\sigma_\theta^2[1 - \rho_h(\Delta\xi, \Delta\eta)]\} . \tag{2.169}$$

This result provides us with a specific relationship between the correlation properties of the reflected fields and the correlation properties of the reflecting surface. If the normalized correlation function of the surface heights is also of Gaussian form,

$$\rho_h(r) = \exp\left[-\left(\frac{r}{r_c}\right)^2\right], \tag{2.170}$$

where $r=\sqrt{(\Delta\xi)^2+(\Delta\eta)^2}$, then the complex coherence factor of the fields becomes

$$\mu_\alpha(r)=\exp\left[-\sigma_\theta^2(1-e^{-(r/r_c)^2})\right]. \tag{2.171}$$

This function is plotted in Fig. 2.24 for various values of phase variance σ_θ^2. For large separations r, $\mu_\alpha(r)$ approaches a non-zero asymptote $\exp(-\sigma_\theta^2)$, indicating that the reflected wave has a non-zero mean value. This mean reflected wave corresponds to the specular component of

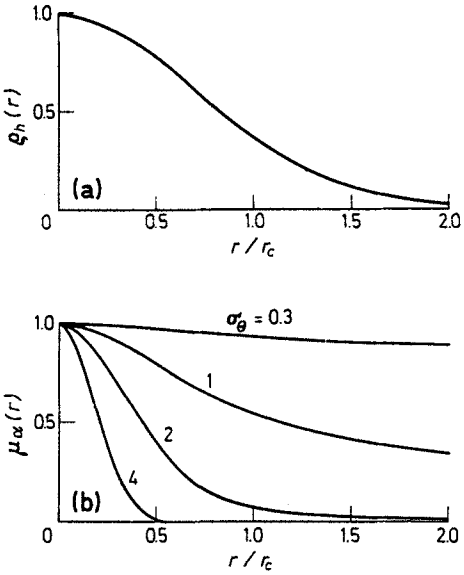

Fig. 2.24a and b. Plots of (a) the assumed correlation function of the surface and (b) the corresponding complex coherence factor of the fields at the surface for several values of σ_θ^2

reflection and has significant value only when $\sigma_\theta^2 \gtrsim 1$. We further note that for large σ_θ^2, the width of $\mu_\alpha(r)$ is much narrower than the width of ρ_h, indicating that the coherence area of the reflected wave is far smaller than the correlation area of the surface. Thus for large σ_θ^2, the coherence properties of the reflected wave depend only on the behavior of the surface correlation function near the origin.

If we subtract out the specular component and re-normalize for value unity at $r=0$, we obtain a normalized correlation function of the reflected wave

$$\rho_\alpha(r)=\frac{\exp\left[-\sigma_\theta^2(1-e^{-(r/r_c)^2})\right]-\exp(-\sigma_\theta^2)}{1-\exp(-\sigma_\theta^2)}. \tag{2.172}$$

For some purposes it may be useful to have an expression for the coherence area of the non-specular component of the reflected wave. The definition

$$S_c \doteq 2\pi \int_0^\infty r|\rho_\alpha(r)|\,dr \tag{2.173}$$

turns out to be simple and yields physically appealing results.

To calculate S_c, we substitute (2.172) in (2.173) with the result

$$S_c = \frac{2\pi e^{-\sigma_\theta^2}}{1-\exp(-\sigma_\theta^2)} \int_0^\infty r\left[\exp(\sigma_\theta^2 e^{-(r/r_c)^2}) - 1\right] dr\,. \tag{2.174}$$

Expanding the outer exponential in a power series, we find

$$S_c = \frac{2\pi e^{-\sigma_\theta^2}}{1-\exp(-\sigma_\theta^2)} \sum_{k=1}^{\infty} \frac{(\sigma_\theta^2)^n}{n!} \int_0^\infty r e^{-n(r/r_c)^2} dr\,. \tag{2.175}$$

The integral equals $r_c^2/2n$, and hence

$$S_c = \frac{\pi r_c^2 e^{-\sigma_\theta^2}}{1-\exp(-\sigma_\theta^2)} \sum_{k=1}^{\infty} \frac{(\sigma_\theta^2)^n}{n \cdot n!}\,. \tag{2.176}$$

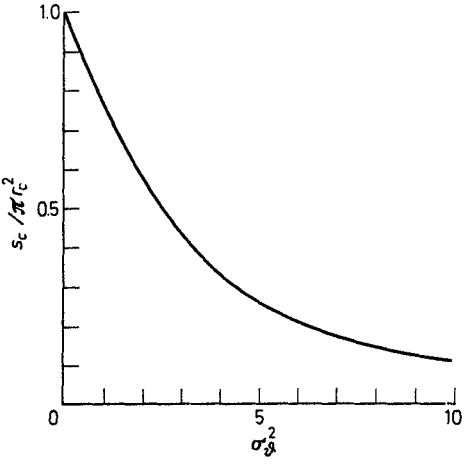

Fig. 2.25. Ratio of correlation area S_c of the reflected wave to πr_c^2 as a function of σ_ϑ^2

Finally, the series can be summed [Ref. 2.54, p. 229], yielding the result

$$S_c = \pi r_c^2 \frac{e^{-\sigma_\theta^2}}{1-\exp(-\sigma_\theta^2)} [\mathrm{Ei}(\sigma_\theta^2) - \mathscr{C} - \ln \sigma_\theta^2] \tag{2.177}$$

where Ei(···) represents the exponential integral and $\mathscr{C}$ is Euler's constant.

In Fig. 2.25, the normalized coherence area $S_c/\pi r_c^2$ is plotted vs. the phase variance σ_θ^2. For small $\sigma_\theta^2, S_c/\pi r_c^2$ asymptotically approaches unity, while for large σ_θ^2 it asymptotically approaches σ_θ^{-2}. Clearly for large σ_θ^2, the coherence area of the reflected wave is much smaller than the correlation area of the surface itself.

2.7.3 Dependence of Speckle Contrast on Surface Roughness

In this final section, we consider some first-order statistical properties of speckle and their dependence on surface roughness. The geometry considered is chosen to be analogous with that of the experiments of FUJII and ASAKURA [2.51], the only difference being that a reflection geometry is used here, whereas their geometry was for transmission. With reference to Fig. 2.26, the rough surface is illuminated by a normally incident plane wave via the beam splitter BS. Lenses L_1 and L_2 form a two-lens imaging system (z is one focal length), and the speckle is examined in the output plane. Of particular interest will be the contrast $C = \sigma_I/\langle I \rangle$ observed in the speckle plane, and its dependence on surface roughness.

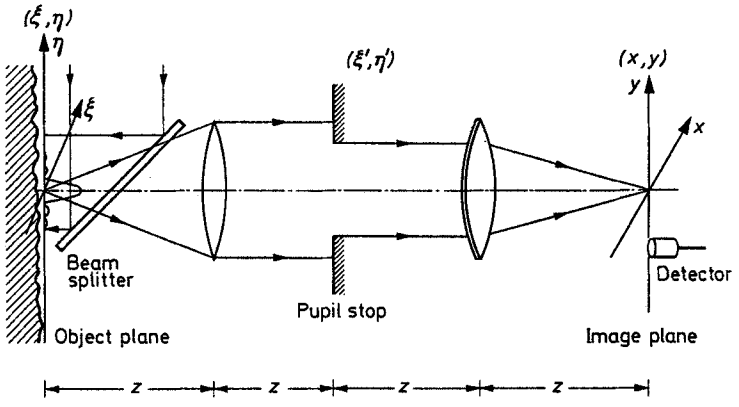

Fig. 2.26. Geometry for contrast measurement

The phase of the light in the object plane (ξ,η) immediately to the right of the reflecting surface is taken to be

$$\theta(\xi,\eta) = \frac{4\pi}{\lambda} h(\xi,\eta), \tag{2.178}$$

and accordingly the phase variance is

$$\sigma_\theta^2 = \left(\frac{4\pi}{\lambda}\right)^2 \sigma_h^2 . \tag{2.179}$$

Since the contrast is of primary concern, we can, without loss of generality, set the reflectivity and the incident intensity equal to unity. Thus the reflected field is taken to be of the form

$$\alpha(\xi,\eta) = \exp\left[i \frac{4\pi}{\lambda} h(\xi,\eta) \right]. \tag{2.180}$$

Assuming that L_1 and L_2 have equal focal lengths, producing a magnification of unity, the field at image coordinates (x,y) is related to $\alpha(\xi,\eta)$ by the convolution equation

$$A(x,y) = \int_{-\infty}^{\infty}\int K(x-\xi, y-\eta)\alpha(\xi,\eta)\, d\xi\, d\eta \tag{2.181}$$

where $K(\cdots)$ represents an amplitude weighting function in the (ξ,η) plane. This weighting function can be expressed in terms of the pupil function $k(\xi',\eta')$ in the pupil plane by

$$K(\xi,\eta) = \frac{1}{\lambda z} \int_{-\infty}^{\infty}\int k(\xi',\eta') \exp\left[i \frac{2\pi}{\lambda z} (\xi\xi' + \eta\eta') \right] d\xi'\, d\eta' \tag{2.182}$$

where k has the property that

$$|k| = \begin{cases} 1 & (\xi',\eta') \text{ in the pupil} \\ 0 & \text{otherwise.} \end{cases} \tag{2.183}$$

For most pupil apertures of interest, $K(\xi,\eta)$ is a real-valued function, a property we shall make use of.

If the weighting function $K(\xi,\eta)$ extends over an area that is large compared with the coherence area of $\alpha(\xi,\eta)$, then to an excellent approximation the real and imaginary parts of $A(x,y)$ will obey Gaussian

statistics, a consequence of the central limit theorem. If in addition we assume that the surface height function $h(\xi,\eta)$ is a zero-mean Gaussian random process, we can prove two important properties of the field A. First, its real part has a non-zero mean value, corresponding to the specular component of the scattered light. Second, the diffuse component of A is *not* a circular complex random variable.

Consider first the mean values of the real and imaginary parts of the field $A(x,y)$. Noting that $K(\xi,\eta)$ has been assumed real-valued, we have

$$\begin{aligned}\langle A^{(r)}\rangle &= \int_{-\infty}^{\infty}\int K(x-\xi,y-\eta)\langle\cos\theta(\xi,\eta)\rangle\,d\xi\,d\eta \\ &= \lambda z\exp\left(-\frac{\sigma_\theta^2}{2}\right), \qquad (2.184)\\ \langle A^{(i)}\rangle &= \int_{-\infty}^{\infty}\int K(x-\xi,y-\eta)\langle\sin\theta(\xi,\eta)\rangle\,d\xi\,d\eta = 0\,,\end{aligned}$$

where we have used the facts that

$$\int_{-\infty}^{\infty}\int K(\xi,\eta)\,d\xi\,d\eta = \lambda z k(0,0) = \lambda z \qquad (2.185)$$

and that θ is a zero mean stationary Gaussian random process.

As for the second moments, we can show with the help of (2.169) and some straightforward manipulations that

$$\begin{aligned}\langle[A^{(r)}]^2\rangle &= \mathrm{e}^{-\sigma_\theta^2}\int_{-\infty}^{\infty}\int \mathscr{K}(\Delta\xi,\Delta\eta)\cosh\left[\sigma_\theta^2\,\rho_h(\Delta\xi,\Delta\eta)\right]d\Delta\xi\eta\,,\\ \langle[A^{(i)}]2\rangle &= \mathrm{e}^{-\sigma_\theta^2}\int_{-\infty}^{\infty}\int \mathscr{K}(\Delta\xi,\Delta\eta)\sinh\left[\sigma_\theta^2\,\rho_h(\Delta\xi,\Delta\eta)\right]d\Delta\xi\,d\Delta\eta\,,\\ \langle A^{(r)}A^{(i)}\rangle &= 0\,, \qquad (2.186)\end{aligned}$$

where

$$\mathscr{K}(\Delta\xi,\Delta\eta) \doteq \int_{-\infty}^{\infty}\int K(\xi_1,\eta_1)K(\xi_1-\Delta\xi,\eta_1-\Delta\eta)\,d\xi_1\,d\eta_1\,, \qquad (2.187)$$

while $\cosh[\cdots]$ and $\sinh[\cdots]$ represent hyperbolic cosine and hyperbolic sine, respectively. Subtracting off the squared mean of $A^{(r)}$ to find the

variances, and noting that $\mathscr{K}(\Delta\xi,\Delta\eta)$ is to a good approximation equal to $\mathscr{K}(0,0)$ over the range of $(\Delta\xi,\Delta\eta)$ for which the rest of the integral has value, we obtain

$$\begin{aligned}\sigma_r^2 &= e^{-\sigma_\theta^2}\mathscr{K}(0,0)\int_{-\infty}^{\infty}\int\{\cosh[\sigma_\theta^2\rho_h(\Delta\xi,\Delta\eta)]-1\}\,d\Delta\xi\,d\Delta\eta\\ \sigma_i^2 &= e^{-\sigma_\theta^2}\mathscr{K}(0,0)\int_{-\infty}^{\infty}\int\sinh[\sigma_\theta^2\rho_h(\Delta\xi,\Delta\eta)]\,d\Delta\xi\,d\Delta\eta\,.\end{aligned} \tag{2.188}$$

An additional simplification is possible by noting that

$$\mathscr{K}(0,0) = \int_{-\infty}^{\infty}\int K^2(\xi,\eta)\,d\xi\,d\eta = \int_{-\infty}^{\infty}\int k^2(\xi',\eta')\,d\xi'\,d\eta' = S_p \tag{2.189}$$

where S_p is the area of the pupil.

The results presented in (2.186) and (2.188) demonstrate that $A^{(r)}$ and $A^{(i)}$ are uncorrelated but have unequal variances. Hence the diffuse component of field is *not* a circular complex random variable. It is of some interest to find asymptotic values of σ_r^2 and σ_i^2 for σ_θ^2 small and large, and hence to determine the departure from circularity in these two limiting cases. For small σ_θ^2 we have

$$\begin{aligned}&\cosh[\sigma_\theta^2\rho_h(\Delta\xi,\Delta\eta)]\cong 1\\ &\sinh[\sigma_\theta^2\rho_h(\Delta\xi,\Delta\eta)]\cong\sigma_\theta^2\rho_h(\Delta\xi,\Delta\eta)\end{aligned} \tag{2.190}$$

and with the help of the definition

$$S_0 \doteq \int_{-\infty}^{\infty}\int\rho_h(\Delta\xi,\Delta\eta)\,d\Delta\xi\,d\Delta\eta \tag{2.191}$$

for the correlation area of the surface itself, we find

$$\begin{aligned}&\sigma_r^2\cong 0\\ &\sigma_i^2\cong\sigma_\theta^2 S_0 S_p\end{aligned} \tag{2.192}$$

Thus the statistics the diffuse component of field are highly non-circular for small σ_θ^2.

For large σ_θ^2, we use the asymptotic properties

$$\begin{aligned}&\cosh[\sigma_\theta^2\rho_h(\Delta\xi,\Delta\eta)]\cong\tfrac{1}{2}\exp[\sigma_\theta^2\rho_h(\Delta\xi,\Delta\eta)]\\ &\sinh[\sigma_\theta^2\rho_h(\Delta\xi,\Delta\eta)]\cong\tfrac{1}{2}\exp[\sigma_\theta^2\rho_h(\Delta\xi,\Delta\eta)]\end{aligned} \tag{2.193}$$

to obtain the result

$$\sigma_r^2 \cong \sigma_i^2 = S_p \frac{e^{-\sigma_\theta^2}}{2} \int\int_{-\infty}^{\infty} \exp\left[\sigma_\theta^2 \rho_h(\Delta\xi, \Delta\eta)\right] d\Delta\xi \, d\Delta\eta \,. \tag{2.194}$$

Thus in the limit of large phase variance, circularity of the statistics is restored. Note our conclusions in these two limiting cases hold regardless of the correlation function ρ_h of the surface.

Solutions for σ_r^2 and σ_i^2 can be found for an arbitrary σ_θ^2 once a specific form for ρ_h is adopted. We choose the two-dimensional Gaussian form of (2.170). Expanding the integrands of (2.188) in a series and integrating term-by-term (c.f., (2.175) and (2.176)) we find

$$\begin{aligned} \sigma_r^2 &= S_p \pi r_c^2 e^{-\sigma_\theta^2} \sum_{n=1}^{\infty} \frac{(\sigma_\theta^2)^{2n}}{2n(2n)!} = \left[\mathrm{Chi}(\sigma_\theta^2) - \mathscr{C} - \ln \sigma_\theta^2\right] \\ \sigma_i^2 &= S_p \pi r_c^2 e^{-\sigma_\theta^2} \sum_{n=0}^{\infty} \frac{(\sigma_\theta^2)^{2n+1}}{(2n+1)(2n+1)!} = \mathrm{Shi}(\sigma_\theta^2) \,, \end{aligned} \tag{2.195}$$

where Chi(···) and Shi(···) are the hyperbolic cosine and sine integrals, respectively, [Ref. 2.54, p. 232], and $\mathscr{C}$ is again Euler's constant.

Attention is now turned to the contrast of the speckle pattern and its dependence on surface roughness. Since $A^{(r)}$ and $A^{(i)}$ are approximately Gaussian, we can show (with a modest amount of algebra) that

$$\sigma_I^2 = 4 I_s \sigma_r^2 + 2\sigma_r^4 + 2\sigma_i^4 \tag{2.196}$$

where I_s is the intensity of the specular component. In addition, it is straightforward to show that

$$\langle I \rangle = I_s + \sigma_r^2 + \sigma_i^2 \,. \tag{2.197}$$

Thus the contrast of the speckle must be given by

$$C = \frac{\sigma_I}{\langle I \rangle} = \frac{\sqrt{4 I_s \sigma_r^2 + 2\sigma_r^4 + 2\sigma_i^4}}{I_s + \sigma_r^2 + \sigma_i^2} \tag{2.198}$$

If the diffuse component of scattered field had circular statistics ($\sigma_r^2 = \sigma_i^2 = \sigma^2$), as assumed by PEDERSON [2.52], the result would have been

$$C = \frac{\sqrt{4 I_s \sigma^2 + 4\sigma^4}}{I_s + 2\sigma^2} \,. \tag{2.199}$$

If we now incorporate (2.195), we obtain the following expression for the contrast

$$C = \frac{\left\{\frac{4}{N}[\mathrm{Chi}\,\sigma_\theta^2 - \mathscr{C} - \ln\sigma_\theta^2] + \frac{2}{N^2}[(\mathrm{Chi}\,\sigma_\theta^2 - \mathscr{C} - \ln\sigma_\theta^2)^2 + (\mathrm{Shi}\,\sigma_\theta^2)^2]\right\}^{1/2}}{1 + \frac{1}{N}[\mathrm{Ei}(\sigma_\theta^2) - \mathscr{C} - \ln\sigma_\theta^2]}. \tag{2.200}$$

Here the parameter N is defined by

$$N = \frac{\lambda^2 z^2}{S_p \pi r_c^2} \tag{2.201}$$

and represents the number of correlation areas of the surface that contribute to the observed intensity. This function is shown, for several values of N, by the solid lines of Fig. 2.27. For sufficiently large σ_θ, the speckle contrast saturates at its "rough surface" value of unity. For small σ_θ, the contrast behaves asymptotically as

$$C \cong \frac{\sigma_\theta^2}{\sqrt{N}} \qquad (\sigma_\theta^2 \ll 1), \tag{2.202}$$

a result which differs from that of PEDERSON [2.52] due to his use of circular complex Gaussian statistics. For comparison purposes, the dotted curves of Fig. 2.27 show the dependence of contrast on σ_θ when the

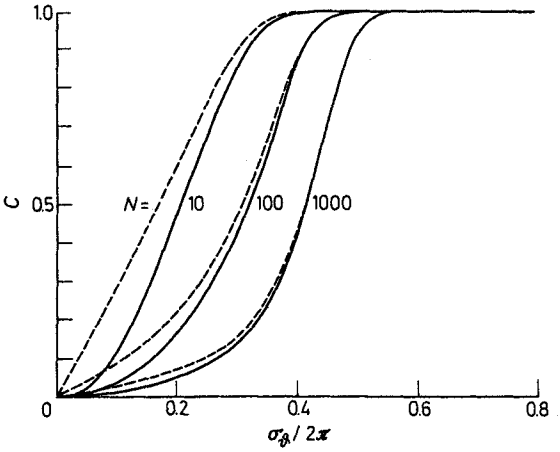

Fig. 2.27. Speckle contrast as a function of rms phase deviation, Gaussian surface correlation function assumed

statistics are assumed circular. Noncircularity is seen to be most important when σ_θ is small, and it is precisely under this condition that information regarding surface roughness is most readily obtainable from the contrast. However, recent experimental results of OHTSUBO and ASAKURA [2.55] can be interpreted as indicating that circularity of the statistics is violated only in the immediate vicinity of the image plane. Thus PEDERSON's results appear to be correct in all cases except the imaging geometry.

Acknowledgement

Portions of the author's own research reported herein were sponsored by the Office of Naval Research. For assistance with numerical computations, thanks are given to: D. JOYEUX, of the Institut d'Optique, Orsay, France; R. POWERS, Stanford Electronics Laboratories, Stanford, California; and R.C. SMITH, University of West Florida, Pensacola, Florida.

References

2.1 J.D. RIGDEN, E.I. GORDON: Proc. I.R.E. **50**, 2367 (1962)
2.2 B.M. OLIVER: Proc. IEEE **51**, 220 (1963)
2.3 E. VERDET: Ann. Scientif. l'Ecole Normale Supérieure **2**, 291 (1865)
2.4 J.W. STRUTT (Lord Rayleigh): Phil. Mag. **10**, 73 (1880)
2.5 M. VON LAUE: Sitzungsber. Akad. Wiss. (Berlin) **44**, 1144 (1914); M. VON LAUE: Mitt. Physik Ges. (Zürich) **18**, 90 (1916); M. VON LAUE: Verhandl. Deut. Phys. Ges. **19**, 19 (1917).
2.6 P.E. GREEN: In *Radar Astronomy*, ed. by J.V. EVANS and T. HAGFORS (McGraw Hill Book Co., New York 1968)
2.7 E.N. LEITH: Proc. IEEE **59**, 1305 (1971)
2.8 P.S. GREEN: *Acoustical Holography*, Vol. 5 (Plenum Press, New York, N.Y. 1974)
2.9 J.A. RATCLIFFE: In *Reports on Progress in Physics*, Vol. 19, ed. by A.C. STRICKLAND (Physical Society, London 1956)
2.10 L. MANDEL: Proc. Phys. Soc. **74**, 233 (1959)
2.11 D. MIDDLETON: *Introduction to Statistical Communication Theory* (McGraw Hill Book Co., New York 1960)
2.12 W.B. DAVENPORT, W.L. ROOT: *Random Signals and Noise* (McGraw Hill Book Co., New York 1958)
2.13 J.W. GOODMAN: Stanford Electronics Laboratories TR2303-1 (SEL-63-140) (1963)
2.14 P. BECKMANN, A. SPIZZICHINO: *The Scattering of Electromagnetic Waves from Rough Surfaces* (Pergamon/Macmillan, London, New York 1963)
2.15 K. PEARSON: *A. Mathematical Theory of Random Migration* (Draper's Company Research Memoirs, Biometric Series III, London 1906)
2.16 J.W. STRUTT (Lord Rayleigh): Phil. Mag. **37**, 321 (1919)
2.17 J.W. GOODMAN: Proc. IEEE **53**, 1688 (1965)
2.18 J.W. STRUTT: Proc. Lond. Math. Soc. **3**, 267 (1871)
2.19 M.A. CONDIE: An Experimental Investigation of the Statistics of Diffusely Reflected Coherent Light, Thesis (Dept. of Electr. Engng.) Stanford University, Stanford, Calif. (1966)

2.20 J.C. DAINTY: Opt. Acta **17**, 761 (1970)
2.21 T.S. MCKECHNIE: Optic **39**, 258 (1974) and thesis, University of London (1975)
2.22 M. FRANCON: Opt. Acta **20**, 1 (1973)
2.23 E. ARCHBOLD, A.E. Ennos, P.A. Taylor: In *Optical Instruments and Techniques*, ed. by J. HOME-DICKSON (Oriel Press, Newcastle-upon-Tyne 1970)
2.24 J.W. GOODMAN: Opt. Commun. **13**, 244 (1975)
2.25 I.S. REED: IRE Trans. Information Theory *IT*-**8**, 194 (1962)
2.26 D.C. MURDOCH: *Linear Algebra for Undergraduates* (John Wiley & Sons, New York 1957)
2.27 R. BARAKAT: Opt. Acta **20**, 729 (1973)
2.28 E. WOLF: Nuovo Cimento **13**, 1165 (1959)
2.29 R.C. JONES: J. Opt. Soc. Am. **31**, 488, 500 (1941)
2.30 J.M. BURCH: In *Optical Instruments and Techniques* ed. by HOME-DICKSON (Oriel Press, Newcastle-upon Tyne 1970)
2.31 J.W. GOODMAN: J. Opt. Soc. Am **57**, 493 (1967)
2.32 D. VILKOMERSON: J. Opt. Soc. Am **61**, 929 (1971)
2.33 W.H. LEE: J. Opt. Soc. Am. **62**, 797 (1972)
2.34 J.C. DAINTY: J. Opt. Soc. Am. **62**, 595 (1972)
2.35 J.I. MARCUM: IRE Trans. Information Theory IT-**6**, 59 (1960)
2.36 E. WOLF: Proc. Roy. Soc. (London) A **225**, 96 (1954)
2.37 J.W. GOODMAN: *Introduction to Fourier Optics* (McGraw-Hill Book Co., New York 1968)
2.38 M. BORN, E. WOLF: *Principles of Optics*, 4th ed. (Pergamon Press, London, New York 1970)
2.39 L.I. GOLDFISCHER: J. Opt. Soc. Am. **55**, 247 (1965)
2.40 S. LOWENTHAL, H.H. ARSENAULT: J. Opt. Soc. Am. **60**, 1478 (1970)
2.41 F. ZERNIKE: Physica **5**, 785 (1938)
2.42 S.O. RICE: In *Selected Papers on Noise and Stochastic Processes*, ed. by N. WAX (Dover Press, New York 1954)
2.43 J.C. DAINTY: Opt. Acta **18**, 327 (1971)
2.44 A.A. SCRIBOT: Opt. Commun. **11**, 238 (1974)
2.45 J. MEIXNER, F.W. SCHAEFKE: *Mathieusche Funktionen und Sphäroidfunktionen* (Springer Berlin, Göttingen, Heidelberg 1954)
2.46 D. SLEPIAN: Bell Syst. Tech. **37**, 163 (1958)
2.47 B.R. FRIEDEN: In *Progress in Optics*, Vol. IX, ed. by E. WOLF (North-Holland Publishing Co., Amsterdam 1971)
2.48 R.B. CRANE: J. Opt. Soc. Am. **60**, 1658 (1970)
2.49 H.H. ARSENAULT: J. Opt. Soc. Am. **61**, 1425 (1971)
2.50 J.W. GOODMAN: In *Remote Techniques for Capillary Wave Measurement*, ed. by K.S. KRISHNAN and N. A. PEPPERS (Stanford Research Inst. Rep., Stanford, Calif. 1973)
2.51 H. FUJI, T. ASAKURA: Opt. Commun. **11**, 35 (1974)
2.52 H.M. PEDERSON: Opt. Commun. **12**, 156 (1974)
2.53 F. BERNY, C. IMBERT: Bulletin BNM **11**, 14 (1973)
2.54 M. ABRAMOWITZ, I.A. STEGUN: *Handbook of Mathematical Functions* (Dover Publications, Inc., New York 1965)
2.55 J. OHTBUTSO, T. ASAKURA: Opt. Commun. **14**, 30 (1975)
2.56 G. SCHIFFNER: Dr. dissertation, Technical University of Vienna (1966); also Proc. IEEE **53**, 245 (1965)